



# Olfactory Evidence Accumulation in Mice

## Citation

Wu, Hao. 2021. Olfactory Evidence Accumulation in Mice. Doctoral dissertation, Harvard University Graduate School of Arts and Sciences.

## Permanent link

<https://nrs.harvard.edu/URN-3:HUL.INSTREPOS:37368438>

## Terms of Use

This article was downloaded from Harvard University's DASH repository, and is made available under the terms and conditions applicable to Other Posted Material, as set forth at <http://nrs.harvard.edu/urn-3:HUL.InstRepos:dash.current.terms-of-use#LAA>

## Share Your Story

The Harvard community has made this article openly available.  
Please share how this access benefits you. [Submit a story](#).

[Accessibility](#)

HARVARD UNIVERSITY  
Graduate School of Arts and Sciences




DISSERTATION ACCEPTANCE CERTIFICATE

The undersigned, appointed by the  
Department of Chemistry & Chemical Biology  
have examined a dissertation entitled:


Olfactory Evidence Accumulation in Mice

presented by: Hao Wu

candidate for the degree of Doctor of Philosophy and hereby  
certify that it is worthy of acceptance.

Signature   
Typed name: Professor Venkatesh Murthy

Signature   
Typed name: Professor Naoshige Uchida

Signature   
Typed name: Professor Hongkun Park

Date: 29 April 2021

Olfactory Evidence Accumulation in Mice

A dissertation presented

by

Hao Wu

to

The Department of Chemistry and Chemical Biology

in partial fulfillment of the requirements

for the degree of

Doctor of Philosophy

in the subject of

Chemistry

Harvard University

Cambridge, Massachusetts

April 2021

© 2021 Hao Wu

All rights reserved.

## **Olfactory Evidence Accumulation in Mice**

### **Abstract**

In nature, odor cues from distant objects are sparse and highly fluctuating due to turbulent airflow. Animals may integrate odor concentration sampled over time rather than rely on transient odor concentration to effectively locate an object. To study how animals integrate and weigh discrete olfactory evidence over time, I developed a new behavioral task in which mice make binary decisions under fluctuating odor stimuli over many seconds. A custom-built device allowed the precise delivery of discrete, short pulses of odors at arbitrary Poisson-distributed pulse rates. I found that trained mice can readily differentiate stochastic odor stimuli with different average pulse rates presented over many seconds. In order to investigate how active, discrete sniff-based sampling of a stochastically varying environmental cue affects the neural representation and perceptual interpretation of the cue, calcium imaging in the axon terminals of olfactory sensory neurons (OSNs) in the glomeruli of olfactory bulb (OB) was performed. I discovered that OSN activity was highly modulated by the phase of the sniffing cycle. Regression of behavioral outcome against the timing of odor pulses in the breathing cycle revealed a kernel that weighted pulses arriving during the inhalation cycle more than during exhalation. This kernel matched the OSN activity kernel over breathing cycle, suggesting that the strength of the perception elicited by single pulses was directly related to the strength of the OSN responses. Decision noise scaled with the number of pulses presented. Tetrode recordings of single-unit neural activities in the anterior piriform cortex (APC) showed high correlations with transient odor pulses, but not the accumulated evidence. The neural activities in APC exhibited diverse dependency on the phase of sniffing, ranging from being strongly modulated by the sniff cycles to sniff-cycle invariant. My

study indicates that mice integrate discrete olfactory inputs over several seconds to make decisions and that perceptual evidence is weighted by the intensity of the OSN response to the input. Furthermore, the platform described in this dissertation introduces a new paradigm in perceptual decision-making in which I can, unlike in vision or audition, record neural activity at all levels, from the first layer of sensory neurons to the decision-making networks.

# Table of Contents

<b>Title</b> .....	<b>i</b>
<b>Copyright</b> .....	<b>ii</b>
<b>Abstract</b> .....	<b>iii</b>
<b>Table of Contents</b> .....	<b>v</b>
<b>List of Figures</b> .....	<b>viii</b>
<b>Acknowledgements</b> .....	<b>xi</b>
<b>1. Introduction</b> .....	<b>1</b>
1.1 Motivation and overview .....	1
1.2 Olfaction-navigation .....	3
1.3 Evidence accumulation .....	5
1.4 Virtual reality experiments in mice .....	8
1.5 The mammalian olfactory system .....	9
1.6 Olfactometers .....	10
1.7 Sniffing and olfactory processing .....	13
1.8 Measuring neural activities .....	15
<b>2. Experimental Methodology</b> .....	<b>17</b>
2.1 Experimental animals .....	17
2.2 Tetrode implantation surgery .....	18

2.3 Electrophysiological recording and analysis .....	18
2.5 Calcium recording .....	20
2.6 Data collection and analysis .....	20
<b>3. Fast Analog Olfactometer .....</b>	<b>22</b>
3.1 Requirement for naturalistic plume simulation .....	22
3.2 Electronic proportional solenoid valve .....	24
3.3 Control circuit .....	27
3.4 Electronic calibration .....	30
3.5 Flow balancing and pulse generation .....	31
3.6 Potential uses of fast analog olfactometer .....	35
<b>4. Sniffing Modulation of Olfactory Sensory Neuron Activities.....</b>	<b>36</b>
4.1 Sniffing and the rate of sniff in head-fixed behavior task .....	36
4.2 Sniffing modulation of OSN activities .....	38
4.3 Phase response curve of odor pulses .....	41
<b>5. Olfactory Evidence Accumulation.....</b>	<b>43</b>
5.1 The Olfactory evidence accumulation training setup .....	43
5.2 The olfactory evidence accumulation task.....	47
5.3 The behavior training sequence and animal learning curve .....	49
5.4 Effects of changing sampling time and pulse-count contrast.....	51



5.5 Weights of evidence across the sampling period .....	52
5.6 Task with Poisson-distributed pulse counts.....	53
5.7 Perceptual weights of evidence .....	55
5.8 Trial history dependency.....	59
5.9 Sources of variability in olfactory evidence accumulation.....	60
5.10 Anterior piriform cortex (APC) recording during evidence accumulation .....	65
5.11 Sniff modulation of anterior piriform cortex (APC) activities.....	69
5.12 Anterior piriform cortex (APC) neural activities represent transient odor information ..	71
5.13 Summary of results .....	73
<b>6. Conclusions and Discussions.....</b>	<b>74</b>
6.1 What is the relationship between the odor concentration and sniffing modulation of OSN response to short odor pulses? .....	74
6.2 Are APC neurons concentration-invariant or concentration-variant? .....	75
6.3 Where is the decision variable (DV) for olfactory evidence accumulation? .....	76
6.4 Is the accumulated evidence utilized in olfaction-based navigation?.....	77
<b>Bibliography .....</b>	<b>78</b>

# List of Figures

1.1 Schematic of chemotaxis .....	3
1.2 Schematic for a simple olfactometer.....	11
3.1 Traditional vs desired odor profile for fast analog olfactometer .....	23
3.2 Example of short odor pulse .....	25
3.3 Example current vs. flowrate profile of EPV.....	26
3.4 Control circuit for EPVs .....	28
3.5 PCB board for the EPV control circuit .....	28
3.6 Heatsink for the EPV control circuit.....	29
3.7 EPV electronic calibration .....	30
3.8 Schematic of the fast analog olfactometer .....	32
3.9 Odor pulse profile from the fast analog olfactometer.....	33
3.10 Example of quickly fluctuating odor profile from the fast analog olfactometer .....	34
4.1 Sniffing flow rate of a mouse during a head-fixed behavior task.....	37
4.2 Distribution of sniff duration during a head-fixed behavior task .....	37
4.3 Calcium imaging of olfactory bulb glomeruli .....	37
4.4 Breathing, odor and GCaMP data during an entire task.....	39
4.5 Comparison of GCaMP data for odor pulses at different timing.....	40

4.6 Phase of sniff.....	42
4.7 Phase response curve of odor pulses.....	42
5.1 The fast olfactometer setup for the olfactory evidence accumulation task.....	44
5.2 Isometric view of the mechanical setup for the evidence accumulation task.....	45
5.3 Side view of the mechanical setup for the evidence accumulation task.....	46
5.4 Example of behavior trials.....	48
5.5 Demonstration of moving lickports.....	48
5.6 Learning curve.....	50
5.7 Performance matrix for sampling time and pulse-count contrast.....	51
5.8 Weights of evidence across sampling period.....	52
5.9 Distribution of trials with different numbers of pulses.....	54
5.10 Psychometric curve for olfactory evidence accumulation.....	54
5.11 Schematic for phase histogram generation.....	56
5.12 Phase response curve of weights of evidence odor pulse timing.....	56
5.13 Correlation between OSN response and weight of evidence.....	57
5.14 Logistic regression weight of decision history.....	58
5.15 Prediction accuracy of different logistic regression models.....	59
5.16 Example of simple gaussian model for behavior variability.....	60

5.17 Sources of variabilities model.....	61
5.18 Scaling of pulse estimation variance.....	62
5.19 Model fit comparison to the psychometric curves.....	63
5.20 Fitted parameters in the sources of variability model .....	64
5.21 Example of single-unit activities in APC during trials.....	66
5.22 Example for neuronal activity extraction in a trial. ....	67
5.23 Example of neurons responding to odor pulses in a trial.....	67
5.24 Distribution of neurons that respond to a proportion of odor pulses .....	68
5.25 Distribution of odor pulses that triggers a proportion of neuronal responses.....	68
5.26 Sniff phase responses of APC neurons .....	69
5.27 Distribution of sniff phase responses of APC neurons .....	70
5.28 Goodness of fit in recording sessions with different number of neurons .....	71
5.29 Goodness of fit vs. integration time .....	72

## Acknowledgements

First and foremost, I would like to express my deepest gratitude and appreciation to my advisor Professor Venki Murthy. He gave me not only the freedom to explore the scientific questions that truly fascinated me, but also all the guidance, encouragements, and resources I needed to identify and answer those questions. Throughout my PhD, Venki has guided me through the most difficult, important decisions in my career, and was beyond supportive when I went through personal hardships. I feel extremely privileged and fortunate to receive the outstanding mentorship from Venki.

I would like to thank Professor Nao Uchida and Professor Hongkun Park for all the valuable insights and helpful advice provided during my committee meetings.

I would like to thank all the amazing members of the Murthy lab: Stephanie Chang, Rebecca Fisher, Elisa Galliano, Julien Grimaud, Dong Hur, Bo Liu, Vikrant Kapoor, Alice Berners-Lee, Luis Boero, Abby Finkelstein, Siddharth Jayakumar, Souvik Mandal, Nuné Martiros, Paul Masset, Alexander Mathis, Selina Qian, Mostafizur Rahman, Elizabeth Strahman, Konrad Urban, Jenelle Wallace, Sonia Wang and Joseph Zak. Thank you for the stimulating discussions on science, career, and life in general. I miss all the lunch conversations, office chats, and parties we had. The Murthy lab members have made the past four years a truly fun and enjoyable journey.

I would like to thank my teammates on my projects. Vikrant Kapoor discovered the EPV valves and taught me to build my first olfactometer. Siddharth Jayakumar and I built the experimental setup and established the first behavior training protocol for olfactory evidence accumulation. Joseph Zak provided me with OMP-GCaMP mice with cranial windows and together we conducted the calcium imaging experiments. Julien Grimaud implanted the tetrode drives and

taught me how to do tetrode recordings. Countless discussions and brainstorming sessions with Paul Masset led to most of the modeling work in this dissertation. Bahareh Tolooshams and Professor Demba Ba developed the algorithm to extract activities from tetrode recordings. Mostafizur Rahman taught me how to use Neuropixels for the future experiments planned in this dissertation. Stephanie Chang helped me in analyzing the sniffing of mice. I also really enjoyed my time working with Souvik Mandal and Dong Hur studying olfactory tracking behavior of ants.

I would like to thank Gautam Reddy and Professor Massimo Vergassola for their help in behavior modeling, Ed Soucy and Brett Graham for their help in machining, electronics, mechanical designs and neuroengineering.

I would like to thank my undergraduate research advisor Naomi Ginsberg for her excellent mentorship and continuous support, as well as all the Ginsberg lab members. I want to especially thank Craig Hetherington for his support throughout my career, from graduate school applications to post-PhD career plans.

I would like to thank Habib Ahmad and Michael Chen, as well as the Verily team who provided me an amazing internship experience in biomedical engineering. The three months at Verily was one of the most exciting times in my career.

I would like to thank Jane Yang for all her support and understanding when I am finishing up my PhD.

Finally, I would like to thank my parents, and all my friends who were there for me in the past six years. I want to especially thank Linlin Fan, Junhan Su, Sara Rubio and Ranjavati Banerji for their unwavering support that helped me overcome the most difficult challenges during my PhD, I would have never made this far without their help.

# 1. Introduction

## 1.1 Motivation and overview

Animals use different senses to gather information crucial for survival from their surrounding environments. An animal can then use the information it has gathered to infer the location of surrounding elements and make decisions on where it would go. Olfaction, the sense of smell, is among one of the oldest and most utilized senses in differentiating and locating different objects and substances. Animals employ the sense of smell to forage for food, to find mates and to avoid predators (Slotnick 2001). Olfactory cues serve as the primary guide for navigation for many different types of animals, from insects to mammals. With their antenna, ants track pheromone trails laid down by other ants or themselves to arrive at previously found food sources. Moths follow odor plumes when travelling upwind (Wills and Arbas 1991; Riffel et al. 2014) to find mates and flowers. Rats have been trained to track ground-borne odor trails on a treadmill (Khan et al. 2012). Recent study (Gire et al. 2016) indicates that mice can locate food pellets by tracing a strand of continuous odor plumes. Indeed, many animals rely heavily on olfaction when they are navigating.

Air-borne olfactory cues carry information about the locations of odor sources. In an environment with no airflow, the odor molecules emitted by an odor source form a continuous gradient driven by diffusion. In nature, however, such continuous gradient is rarely seen as turbulence in airflow disrupts the odor gradient. Instead, odor plumes become discontinuous, characterized by vanishing concentration at most space and time and short pulses of detectable

concentrations that are distributed randomly across space and time (Celani et al. 2014). The distribution statistics of these short pulses of odor are governed by the distance from the odor source and the wind conditions. Under this scenario, an animal cannot use the transient odor concentration at any given moment to determine the location of an odor source. The animal needs to accumulate odor pulse statistics it has collected over time and space to infer its distance and orientation from the odor source.

Rodents such as rats and mice have been shown to accumulate evidence in visual and auditory tasks (Brunton et al. 2013, Odoemene et al. 2018). Evidence accumulation models has been used to explain the effects of reward history on choices in olfactory decision tasks in rats (Mendonça et al. 2020). Due to limitations in the technology of odor delivery (Brunton 2012), no research has been done on the accumulation of discrete olfactory evidence in a single trial prior to the study described in this thesis. Given that rodents rely primarily on olfaction, as well as the discrete nature of naturalistic odor stimuli, it is of great importance to study and characterize rodents' behavior in olfactory evidence accumulation and their neural encoding of discrete olfactory evidence. My study showcases a novel method for odor delivery which generates extremely short pulses of odor (50ms), mimicking discrete odor detection in a turbulent environment. Combined with operant conditioning of mice as well neural recording methods such as tetrode recording and calcium imaging, I developed a behavior paradigm that studies mice's evidence accumulation behavior of discrete olfactory stimuli as well as the neural correlates of the sensory evidence and the behavior.

In this chapter, I will discuss the relevant neuroscience and engineering background associated with studying olfactory evidence accumulation. Chapter 2 describes the experimental



methods I used in the study. Then in Chapter 3, I will demonstrate a novel odor delivery device that can deliver precisely-controlled odor stimuli with extremely short pulse width and high dynamic range. In Chapter 4, I will show the neural representation of discrete odor pulses in the glomeruli of the olfactory bulb. In Chapter 5, I will describe a novel olfactory evidence accumulation task and characterize the behaviors of mice in this task. In Chapter 6, I will discuss the neural encoding of odor evidence in the piriform cortex. I will then close this thesis with conclusions and discussion for future directions in Chapter 7.

## 1.2 Olfaction-based navigation

Olfaction-based navigation is commonly found in nature. The simplest form of olfaction-based navigation can be found as chemotaxis (Figure 1.1). Chemotaxis is the movement of a single cell or an organism according to a certain chemical gradient, such as nutrient concentration and oxygen level, in its surrounding environment (Stock and Baker 2009). Organisms continuously monitor the sensory information around it to move towards a location that can best grow. In this situation, the chemical gradient is usually continuously changing in space and time.

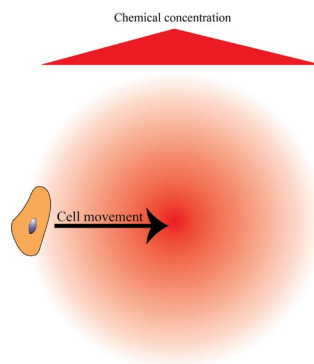


Figure 1.1. Schematic of chemotaxis, a cell could move up or down from chemical gradients.

Another form of olfaction-based navigation is the tracking of trails. Social insects such as ants lay down a continuous line of pheromone trails when they return to home from a food source, so that the other ants can arrive at the same food source following the trail (Klowden 2008). Ants that are following the trail brush their antenna against the trail, and the olfactory receptor neurons (ORN) on their antenna detect the pheromone molecules on the trail (Draft et. al. 2018). This olfactory information guides the movement of ants so that they would stay on the trail. Similar terrestrial trail tracking behavior can be found in rodents. Rats can be trained to accurately follow a continuous, artificial trail on a treadmill, and employ a near-optimal sampling strategy when sniffing around the trail (Khan et al. 2012).

Not all olfactory cues are continuous in space and time. In nature, turbulence in the air and complex landscapes break up the odor stream from an odor source (Figure 1.2). Rather than forming a continuous chemical gradient, or a continuous ribbon of odor plume, the odor molecules travel in discontinuous odor whiffs with similar intensity that are separated by space where odor molecule concentrations are vanishing, so that around a given point in space, the time series of odor concentration are characterized by intermittent, discrete pulses of odors with similar intensities (Celani et al. 2014). The frequency of odor pulses arriving at a certain point is higher for points that are closer to an odor source and lower for points that are further away from an odor source (Celani et al. 2014). Under this condition, an animal that is navigating in an environment using airborne odor cues will need to integrate odor stimuli over time to gather information about its proximity to an odor source instead of following a continuous odor gradient by taking transient odor stimuli inputs.

Moths are well known to utilize sparse odor information over an extremely long range to find mates and food sources (Wills et al. 1991, Riffel et al. 2014). The search behavior of moths in an environment with sparse odor stimuli matches the infotaxis strategy (Vergassola et al. 2007), where the searching agent movement optimizes the expected rate of information gain to climb up an odor concentration gradient. Rodents such as mice travel a large distance when foraging over complex terrains and use olfaction as a guide to navigation. It is of interest to study whether mice could integrate information of discrete odor stimuli over time.

### 1.3 Evidence accumulation

Animals are known to accumulate, or integrate evidence from different sources (e.g. vision, audition, vibrotactile perception) over time in order to guide their decision-making (Gold and Shadlen 2007). Rodents are not the exception. Rats can accumulate evidence from discrete sound clicks and light flashes, and make decisions based on the number of clicks they hear or the flashes they see with no memory noise (Brunton 2012).

In experiments involving discrete sensory stimuli, each discrete sensory input can be seen as a single piece of noisy evidence. Signal detection theory (SDT) can be used to associate the observation of a single piece of noisy evidence to the likelihood that an underlying representation or hypothesis (e.g. stimulus present vs stimulus absent) generates such an evidence (Green and Swets 1966). For evidence accumulation experiments, each trial in the experiments involves a sequence of discrete pieces of evidence. The sequential analysis (SA) framework could then be used to combine the likelihood corresponding to each piece of evidence into the likelihood that a representation generates all the pieces of evidence in a given trial (Gold and Shadlen 2007). The

logarithm of the ratio between the combined likelihoods of two representations, also known as the decision variable (DV), could be calculated by summing the logarithm of the likelihood ratio of each piece of evidence (logLR, or “weight of evidence”). This DV is a value that indicates the relative likelihood that the pieces of evidence arise from one representation or hypothesis vs the other, and could be used to the decision making of an animal receiving such stimuli. One commonly used implementation of SA is the diffusion decision model (DDM, Ratcliff and McKoon 2008), where an animal makes a decision when the DV crosses a certain threshold. DDM is suited for evidence accumulation experiments where the time to decision is controlled by an animal. For evidence accumulation experiments where the time to decision-making is fixed, the decision model could be modified from DDM so that an animal makes a decision based on the DV at the end of the allotted time to decision-making and a certain threshold.

DDM assumes that each piece of evidence is observed and added to the DV independently. This assumption might not be true for some evidence accumulation experiments. Source of noise analysis (Scott et al. 2015) performed on visual and auditory accumulation tasks in rats suggests that a numerical cognition and counting model is more suited because of the linear scaling of decision variability with the number of pieces of evidence.

In the study described by this thesis, I implemented a fixed time to decision-making, and used an adapted version of the source of noise analysis to study how pieces of discrete olfactory evidence are combined to guide the decision making process of mice.

In visual and auditory evidence accumulation tasks, activities associated with the DV and accumulated evidence have been found in the brain regions (Brody and Hanks 2016) such as the frontal and posterior parietal cortex (Scott et al, 2015, Scott et al., 2017), prefrontal cortex (Hanks

et al. 2015), striatum (Yartsev et al., 2018). There has been no prior studies of neural correlates of the DV in olfactory evidence accumulation tasks. Unlike in the visual and auditory systems, sensory neurons in the olfactory systems do not pass direct inputs onto the thalamus. Instead, information of olfactory signals transfers directly from the olfactory bulb to the olfactory cortex. The piriform cortex in the olfactory system contains recurrent connections (Franks et al. 2011). In my study, I investigated whether correlates of the DV or accumulated evidence could be found in the piriform cortex due to its recurrent nature.

## 1.4 Virtual reality experiments in mice

Advances in graphics display and sensor technology have driven the development of virtual reality experiments in mice, where the navigation behavior of animals are investigated in a precisely controlled virtual reality environment where a head-fixed mouse ran on a spherical ball through a virtual maze controlled projected on a screen (Minderer and Harvey 2016). This type of experimental configurations enable scientists to study navigation behaviors of animals in a head-fixed setting, where powerful neural activity recording tools such as 2-photon calcium imaging could be easily used. The experimental stimuli can be precisely controlled and quickly altered in the virtual environment in order to study how neurons react to changes in the environment. A form of evidence accumulation experiment was introduced in the virtual reality configuration, where a mouse was trained to make specific turns in a virtual T-mazed based on the number of pillars it saw on the left and right sides in the virtual corridor (Morcos and Harvey 2016, Pinto et al. 2018).

A virtual reality navigation study (Radvansky and Dombeck 2018) involving continuous varying odor gradient shows that mice could navigate purely based on an ascending or descending

concentration gradient in a dark environment. The study found place cells in hippocampal CA1 that were solely activated by specific segments of the odor concentration gradients. There has been no prior virtual reality studies involving discrete odor stimuli. The setup described in this thesis has the capability to perform virtual reality experiments and enable the possibility of virtual reality navigation tasks in an environment with naturalistic, stochastic odor stimuli.

## 1.5 The mammalian olfactory system

The mammalian olfactory system has been extensively studied and characterized. The system consists of the olfactory sensory neurons (OSN) in the nasal cavity of an animal, the olfactory bulb (OB), the lateral olfactory tract (LOT), and the olfactory cortex (Giessel and Datta 2014). The olfactory cortex encompasses the anterior olfactory nucleus, the piriform cortex (PCTX), the olfactory tubercle (OT) and the cortical amygdala (CoA). In my study, I will focus on the OSN, OB and the PCTX.

OSNs in the nasal cavities have olfactory receptors (OR, Buck and Axel 1991) that bind to odor molecules. There are many different ORs (~1000 in mice, Godfrey et al. 2004) that have different binding affinities to different molecules. Each OSN only expresses a single type of OR (Serizawa et al 2004). After binding to an odor molecule, the OR triggers a GPCR pathway and activates the ORNs (Pifferi et al. 2010, Kleene et al. 2008). The neural activity level of an ORNs, reflected by its firing rate or calcium amplitude, is determined by the concentration of a specific odor (Lansky and Rospars 1998) as well as the presence of other types of odor molecules that is also bounded to the same neuron (Zak et al. 2020).

The OSNs project to the OB, where the axon terminals of OSNs with the same type of ORs are spatially organized into circular regions on the surface of the OB known as olfactory glomeruli (Mombaerts et al 1996, Imai et al. 2010). Specific odor molecules activate a specific set of ORs, which can then be visualized as a spatial map of OB glomeruli (Ressler et al. 1994, Vassar et al. 1994, Mombaerts et al 1996). The OSNs projects to a range of cells in the OB, including periglomerular (PG) cells, superficial short-axon (sSA) cells, the mitral cells and the tufted cells (Nagayama et al. 2014). The mitral and tufted (M/T) cells are projection neurons that project signal further down to other olfactory regions including the olfactory cortex. Granular cells in the OB inhibit M/T cells. M/T have dendrites that run laterally and interact with dendrites of granular cells inhibiting surrounding M/T cells in a process known as lateral inhibition.

The PCTX receives input from the M/T cells in the OB, and is thought to process olfactory sensory information into higher level representations, such as odor object (Wilson and Sullivan 2011), where odors or odor mixtures illicit activities in a unique and spatially dispersed group of neurons of similar group size (Giessel and Datta 2014). Previous studies (Bolding and Franks 2017) shows that a large number of neurons in the PCTX show activities that are invariant to odor concentration, where the increase in firing rate of neurons activated by a certain odor does not change between odor stimuli of different concentration intensities. The recurrent circuitry in the PCTX is believed to stabilize the rate coding of odor across different odor intensities (Bolding and Franks 2018). In this study, I aim to discover whether the recurrent circuitry in PCTX, specifically in the anterior piriform cortex (APC), can also represent accumulated evidence or DV.

## 1.6 Olfactometers

For most studies involving olfactory stimuli, the olfactometer is an essential device. The olfactometer is a device that could deliver controlled airflow carrying a specific concentration of odor molecules to the nose of an animal. The key attributes that determine the capabilities of an olfactometer are the ability to deliver a range of different odors, the ability to control odor concentrations, and the speed of on-off state switching. More complex experiments can be done with increased number of odor chemicals and odor concentration levels. An olfactometer that can turn odor delivery on and off faster can be used to generate naturalistic odor plumes, as well as to study sub-sniff olfactory processing of odors.

The most commonly used olfactometer design (Figure 1.2) consists of a regulated air source, tubing, a vial and a solenoid valve (Walker and O'Connell 1986). The air source could be an air pump, a compressed air tank or compressed air outlet in the laboratory. In the off-state of an olfactometer with a normally-off solenoid valve, a spring pushes a metal-core piston to block the flow path in the valve, so that no air can go through. In the on-state, electrical current in a coil around the metal core lifts up the piston, and the flow path is open. Clean air from the air source passes through a solution containing odor molecules to form an odor-enriched air stream. The air stream then passes through a one-way check valve that only allows air stream in the forward direction to the odor outlet, where the odor is delivered (usually to the nose of the animal). In the off state of the olfactometer, no current is in the coil. The piston in the solenoid valve blocks the flow path. The one-way valve prevents any spontaneous, diffusive odor molecules from reaching the odor outlet.



Multiple parallel channels of flow paths could be built based on the aforementioned simple olfactometer design to form an olfactometer of the capability of many different odors. Because of the relative low price, this olfactometer design is easy-to-build and cost-effective. It also delivers a wide range of odors at the same time. However, the flow rate cannot be controlled, so that each odor channel only allows one odor concentration to be delivered. To change concentration, the odor vial needs to be filled with a solution with different odor concentration. The on-off speed is also low due to the slow response time ( $>30\text{ms}$ ) of mass-market solenoid valves.

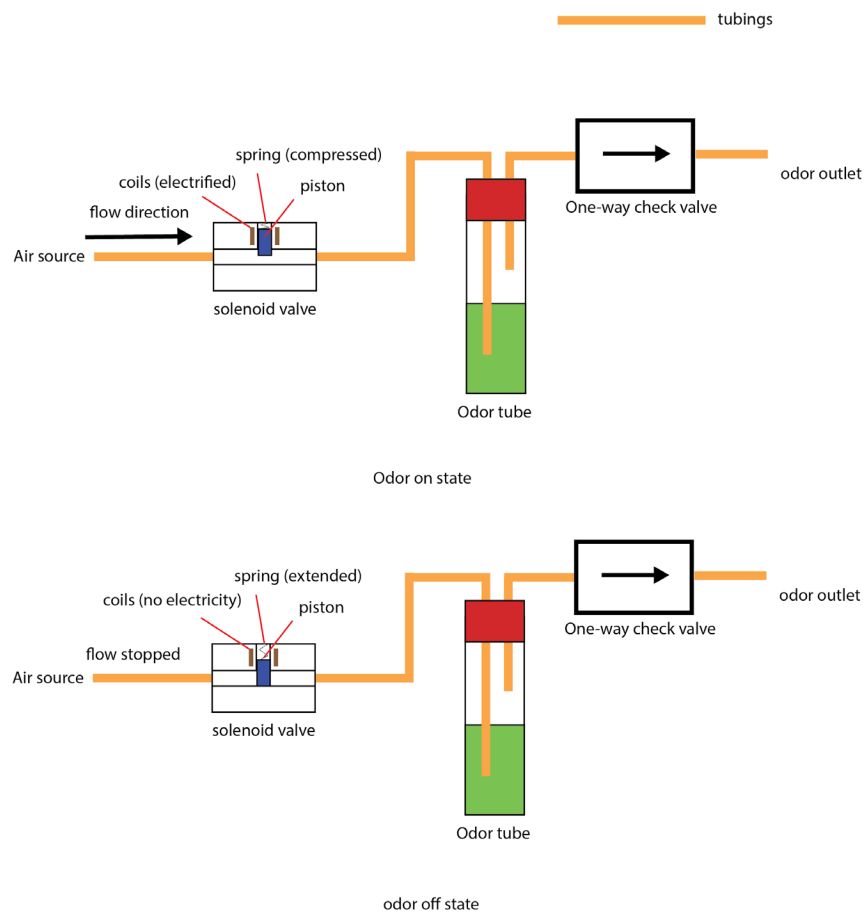


Figure 1.2. Schematic for a simple solenoid based olfactometer design.

An olfactometer design featuring a mass flow controller (MFC) instead of the solenoid can vary the odor concentration of odor delivered (Gupta et al. 2015, Radvansky and Dombeck 2018). The MFC can precisely control the amount of fluid or gas passing through a flow pass, allowing different levels of odor concentrations to be reached. A simpler version of MFC utilizing a stepper motor controlled pinch valve could also achieve similar results. The stepper motor can pincer forward to restrict the opening diameter of a tubing, or backward to increase the opening diameter of the tubing. Because flow rate changes with the diameter of a tubing, changing levels of odor concentration can be achieved. The MFC type of olfactometer design achieves odor delivery of variable concentrations, but is slow due to the long response time of MFCs, stepper motors and pinch valves. When a commercial MFC is used, the setup is also costly (\$2000 per channel).

A third olfactometer design that aims to increase the on-off rate utilizes a specialized solenoid valve with submillisecond on-and-off rate (Erskine et al., 2019). This olfactometer can deliver odor pulses with frequency up to 50Hz (10ms pulse width). This olfactometer design achieves extremely high speed, but could only deliver a specific peak odor pulse concentration.

My study introduces an olfactometer that is capable of delivering many odors with a large range of different odor molecules at the same time with high speed (~20-40Hz) and continuously variable odor concentration. It opens up the possibility to experiment designs with extremely complex odor stimuli, such as a temporal odor profile mimicking naturalistic odor plumes in a turbulent environment.

## 1.7 Sniffing and olfactory processing

Unlike vision and auditory perception, the olfactory sensation of a mammal is modulated by the breathing pattern of the animal. An animal can also perform an active, voluntary intake of air, known as a sniff, to sample odor cues (Wachowiak 2011, Grimaud and Murthy 2018). Each sniff can be viewed as a unit of olfactory processing (Kepecs et al. 2005) and discrete sampling of olfactory cues. Rats could make decisions after taking a single sniff of odors (Uchida and Mainen 2003) and the neural responses to odors are highly conserved in the first 100ms of odor inhalation, regardless of the duration of the sniffing cycle (Cury and Uchida 2010). Each breath or sniff of an animal consists of an inhalation phase and an exhalation phase. Neural responses to odor stimuli were found to be more tightly time-locked to the phase of sniff cycles than to the time after inhalation onset (Shusterman et al. 2011, Miura et al. 2012). During the inhalation phase, air and odor molecules are taken into the animals' nostrils and detected by the olfactory receptors. During exhalation, the air molecules and air are ejected from the nose. Odor molecules adjacent to the outside of nostril are only detected when they arrive during the inhalation phase. Odor molecules arriving at the exhalation phase are not detected by the animal. The neural activities of OSNs reflect this modulation.

It is important to monitor the breathing and sniffing pattern of animals in experiments involving olfactory stimuli. There are many ways to measure sniffing and breathing. Intranasal canula directly measure the pressure inside the nostril of the animal (Verhagen et al. 2007, Wesson et al. 2008) A thermocouple could be placed in one of animals' nostrils to monitor the temperature change inside the nostrils (Angyán and Szirmai 1967, Clarke et al. 1970, Crossland et al. 1977). Air from the exhalation carries the animal's body heat, so changes in temperature in the nostrils

can be converted to the animal's breathing pattern. The thermocouple method is invasive to the animal. A less invasive method involves a mini vest with a strain gauge attached. It wraps around the chest of the mouse and measures the contraction and the expansion of the chest when the mouse is breathing. Though the vest is less invasive than the implant, a mouse might still get uncomfortable with the restriction of clothing on its body.

Facemasks has been used to monitor the breathing of many animals in the past, including humans (Connell 1966, Ferdenzi et al. 2014, Saibene et al. 1978, Waters 1936) and rodents (Youngentob et al. 1987, Sherman et al. 2015, Bolding and Franks 2017). In this work, a 3D-printed face mask is used. The facemask incorporates the olfactometer's odor outlet, a vacuum port and a flowmeter. With 3D printed material designed precisely to fit the profile of the nose of a mouse, the mask ensures that the animal is comfortable and fits tightly around its nose. The flow rate into the vacuum port is balanced with the flow rate from the odor outlet, so that the net flow airflow into the mask is zero when an animal is not present. When an animal's nose is fitted to the mask, the flowmeter measures precisely the flow into and out of the animal's nostrils. This face mask is noninvasive, and integrates odor delivery, odor exhaust and breathing monitoring in one device.

## 1.8 Measuring neural activities

To understand the neural representations of sensory stimuli, decision variables and animal behaviors in the brain, the activities of neurons need to be recorded. Neural activities are reflected electrically by changes in membrane potentials and chemically by the concentration of ions and

molecules inside and outside neurons. Throughout the history of neuroscience, many methods have been developed to measure neural activities based on the physical and chemical properties of neurons. In this study, tetrode recording, high-density microelectrode array (MEA) and calcium imaging are used.

An action potential (AP) is a stereotypical and rapid change (a spike) in membrane potential in a neuron (White 2002). The rate of AP occurrence in a neuron is known as the firing rate of the neuron. The firing rates, as well as the temporal patterns of spikes of neurons have long been known to encode information and representation in the brain (Dayan and Abbott 2001).

Measuring electrical activities of many neurons in the brain is a nontrivial task. The brain is densely packed with large numbers of neurons, and the electrical potential at any given position inside the brain is affected by many neurons adjacent to that region. Tetrode recording (O'Keefe and Reece, 1993; Wilson and McNaughton, 1993) was developed to record and extract single-unit activities of many neurons in a brain region using an approach similar to the solution for the cocktail party problem (McDermott 2009). Principal component analysis (PCA) and clustering allows isolation of single-unit neuronal activity from the electrical recordings on each tetrode. Tetrodes can be implanted deeply into an animal's brain. The tetrode wires are thin (~ 30  $\mu\text{m}$ ) and minimally invasive. However, the weight and building time of tetrode drives increase dramatically with higher number of tetrodes, limiting the number of neurons (~10-20 per session) that a tetrode drive can record in each session.

High-density MEAs such as Neuropixels improve upon the tetrode drives and can record a large number (up to 350 per session) of neurons (Jun et al. 2017). Using modern complementary metal-oxide-semiconductor (CMOS) technology, hundreds of adjacent recording sites are placed

on a thin (~70 um) probe with high density. Unlike the hand-built tetrode drives, the spatial pattern of recording sites of the factory-fabricated high-density probes are pre-determined. The defined spatial pattern as well as the high density of recording sites allow cleaner clustering and extraction of single-unit activities than tetrode drives.

When a neuron fires an action potential, its intracellular calcium concentration increases. Genetically-encoded fluorescent calcium indicators such as GCaMP (Chen et al. 2013) are designed to measure the changes in calcium concentration in neurons. As an imaging-based method, calcium imaging allows researchers to spatially visualize and separate neurons. Cell-type specific imaging of neurons is also possible because of the genetic encoding of the indicators. The caveats of calcium imaging include slow kinetic of the indicators, slow kinetics of change in calcium concentration and low imaging depth due to light scattering in tissues.

## 2. Experimental Methodology

### 2.1 Experimental animals

#### Behavior and electrophysiology:

All animals in the behavior experiments were C57Bl6/J mice acquired from Jackson Laboratory, aged two to four months at the start of experiments. Following implantation of a tetrode drive, a imaging window, or head plate, all mice were housed individually. Behavior, imaging and physiology experiments took place over the course of one to two months. After the completion of all experiments, mice were euthanized and post-mortem histology was performed to confirm the location of electrophysiological recordings.

#### Olfactory bulb imaging:

Adult heterozygous OMP-GCaMP3 mice of both sexes were used in this study. All animals were produced from a breeding stock maintained within Harvard University's Biological Research Infrastructure. All animals were between 20 and 30 g before surgery and singly housed following any surgical procedure. Animals were 2–6 months old at the time of the experiments. All mice used in this study were housed in an inverted 12 h light cycle and fed ad libitum. Animals were housed at  $22 \pm 1$  °C at 30–70% humidity. All the experiments were performed in accordance with the guidelines set by the National Institutes of Health and approved by the Institutional Animal Care and Use Committee at Harvard University.

## 2.2 Tetrode implantation surgery

Mice were anesthetized with an intraperitoneal injection of ketamine and xylazine (100 mg/kg and 10 mg/kg, respectively), then placed in a stereotaxic apparatus. After the skull was cleaned and gently scratched, a custom-made titanium head bar was glued to it. A small craniotomy was performed above the implantation site, before 8 custom-built tetrodes (Chang et al., 2013) were lowered together into the brain (coordinates for APC: antero-posterior 1.6mm, medio-lateral -2.8mm, dorso-ventral 3.4mm; all antero-posterior and medio-lateral coordinates are given relative to Bregma; all dorso-ventral coordinates are given relative to the brain surface). A reference electrode was implanted on the occipital crest. All the mice were implanted in the right hemisphere. The whole system was stabilized with dental cement. Mice were given a week of recovery before any new manipulation.

## 2.3 Electrophysiological recordings and analysis

A week after chronic tetrode implantation, mice were habituated to stay calm on the head-fixed olfactory evidence accumulation setup. During the habituation, water drops occasionally dropped out of two lickports for mice to learn the association between lickports and water rewards. The habituation process typically took three to four days. Brain activity was then recorded once a day, always at the same period of the day, while the animals performed in the task. The mice were awake, head-restrained, and freely-breathing during all the recordings. Since the tetrode headstage allowed for the tetrodes to be finely adjusted up or down, the tetrodes were slightly lowered in the



brain after each recording session (around 40 $\mu$ m deep), ensuring that different neurons were recorded each day. Electrical activity was amplified, filtered (0.3-6kHz), and digitized at 30kHz (Intan Technologies, RHD2132, connected to an Open Ephys board). The position of the tetrodes in the brain was confirmed post-mortem through electrolesion (200 $\mu$ A for 4s per channel). Spikes are clustered using Kilosort 2 and curated manually using Phy (Pachitariu et. al. 2016). Units with more than 1% of their inter spike intervals below 2ms refractory period were discarded. Units displaying large changes of amplitude or waveform during the recording were also discarded.

## 2.4 Olfactory bulb craniotomy

A craniotomy was performed to provide optical access to both olfactory bulbs. OMP-GCaMP3 mice were first anesthetized with an intraperitoneal injection ketamine and xylazine (100 and 10 mg/kg, respectively) and the eyes were covered with petroleum jelly to keep them lubricated. Body temperature was maintained at 37 °C by a heating pad. The scalp was shaved and then opened with a scalpel blade. After thorough cleaning and drying, the exposed skull was gently scratched with a blade, and a titanium custom-made headplate was glued on the scratches with Loctite 404 Quick Set Adhesive. The cranial bones over the OBs were then removed using a 3 mm diameter biopsy punch (Integra Miltex). The surface of the brain was cleared of debris. The surface of the brain was kept moist with artificial cerebrospinal fluid containing in mM (125 NaCl, 5 KCl, 10 Glucose, 10 HEPES, 2 CaCl<sub>2</sub> and 2 MgSO<sub>4</sub> [pH 7.4]) and Gelfoam (Patterson Veterinary). Two 3 mm No. 1 glass coverslips (Warner) were glued together with optical adhesive (Norland Optical Adhesive 61) and adhered to the edges of the vacated cavity in the skull with Vetbond

(3 M). C&B-Metabond dental cement (Parkell, Inc.) was used to cover the headplate and form a well around the cranial window (Zak et al. 2018; Albneau et al. 2018; Zak et al. 2020). After surgery, mice were treated with carprofen (6 mg/kg) every 24 h and buprenorphine (0.1 mg/kg) every 12 h for 5 days. Animals were allowed to recover for at least 3 days.

## 2.5 Calcium imaging

A week after the olfactory bulb craniotomy, mice were habituated to stay calm on the head-fixed olfactory evidence accumulation setup. During the habituation, water drops occasionally dropped out of two lickports for mice to learn the association between lickports and water rewards. The habituation process typically took three to four days. During imaging sessions, The mice were awake, head-restrained, and freely-breathing. A custom built epifluorescent microscope with blue LED, 4x objective (Olympus) and a camera (FLIR Blackfly 3 monochrome) was placed above the animal's head to record GCaMP3 fluorescence images at 10 fps. Short pulses of odor were delivered to the animals by the fast analog olfactometer described in Chapter 3.

## 2.6 Data collection and analysis

Behavioral data were collected at 1kHz during experimental sessions by a custom software written in Python, and stored as time-series of double-precision numbers in HDF5 data format, this includes the animals licking behavior, respiratory and odor pulse information. All computations were done in Python with NumPy, SciPy and Scikit-Learn. The respiration data were

passed through a butterworth lowpass filter with cut-off frequency at 20Hz. Sniffing peaks were identified using the find peak function in SciPy on the filtered respiration data. Linear regression and logistic regression were performed with the Scikit-Learn package in Python. Maximum likelihood estimations (MLE) were performed by maximizing likelihood functions described in Chapter 5 with the minimize function in SciPy under the sequential least square programming method (SLSQP).

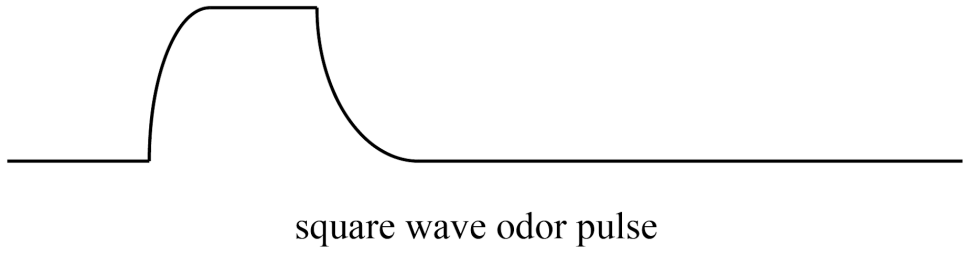
## 3. Fast analog olfactometer

### 3.1 Requirements for naturalistic plume simulation

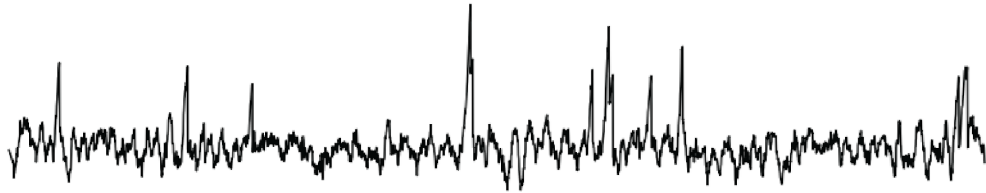
In order to mimic naturalistic odor plumes, an olfactometer needs to satisfy three criteria:

1. The olfactometer delivers a range of different odors so that it can simulate the various odor components of an odor source.
2. The speed of on-off state switching should be high for generating fast odor pulses that are common in a turbulent environment.
3. Precise control of odor concentration level with high dynamic range is desirable to simulate the large distribution of concentration levels in a natural environment.

The most traditional olfactometer design with simple solenoid valve generates odor concentration profile with a long square pulse waveform. The long square pulse mimics odor stimuli in the scenario where an animal is close to an odor source but is far from naturalistic odor stimuli in a turbulent environment (Figure 3.1). Existing methods that address criteria 2 or 3 optimize for only one specific criterion while fail to address the other. Furthermore, mass flow controllers (MFC) and high-speed digital solenoid valves are expensive, which leads to high cost when building multi-channel olfactometers that satisfy criterion 1.



square wave odor pulse



conc.  1s

naturalistic odor profile

Figure 3.1. Traditional vs desired odor profile.

## 3.2 Electronic proportional solenoid valve

The electronic proportional valve (EPV) is a type of solenoid valve that can be used on olfactometers to satisfy criteria 2 and 3 at the same time. EPVs have fast switching time (Figure 3.2) around 5 ms. At closing, a ringing effect leads to turbulent in airflow, leading to a small 20ms tail of odor concentration in a pulse at ~20% of the peak concentration in a odor pulse. The flow rate through the valve can be continuously varied by changing the current amplitude through the solenoid coil (Figure 3.3). EPVs developed by Clippard Corporation are cost-effective (~\$60 per valve), and require ~400mA of current at maximum flow rate. The high speed, variable flow rate and low price make the Clippard EPV valve a great choice as an olfactometer valve.

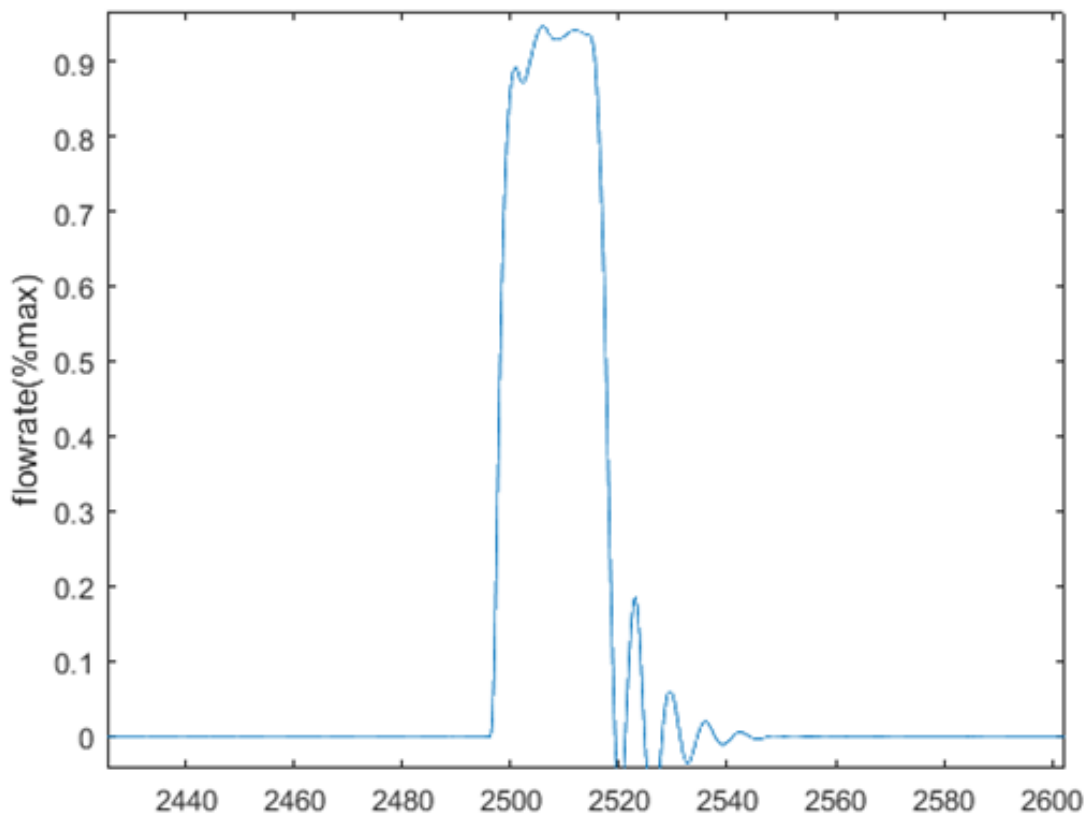


Figure 3.2. An example of a short 20ms pulse of airflow (x-axis has unit in millisecond).

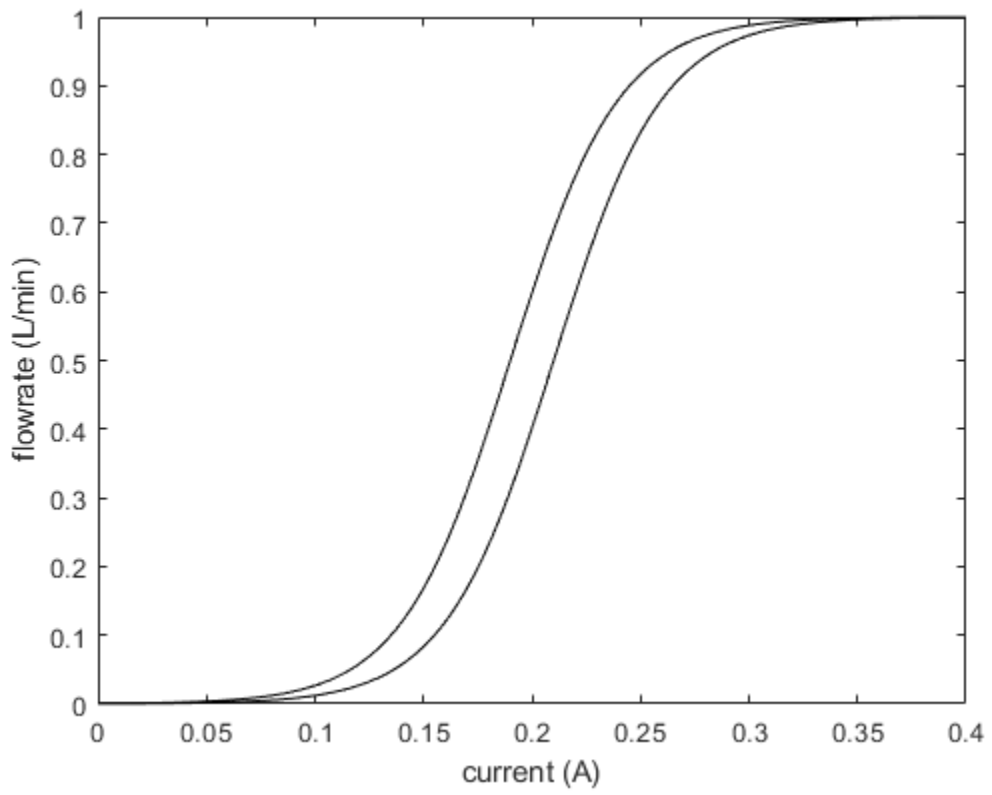


Figure 3.3. Example current vs. flowrate profile of EPV.



### 3.3 Control circuit

Most modern experimental setups output analog commands in the form of voltage. A circuit is needed to convert this variable voltage command to a variable current that matches the current input range of a EPV. A simple electronic circuit (Figure 3.4) consisting of an operational amplifier (opamp), a transistor and a resistor achieves this goal. The inverting input of the opamp monitors the voltage across the resistor, while the non-inverting input of the opamp is connected to the voltage command. The output of the opamp works to match the voltage across the resistor to the voltage command, so that the current passing through the resistor is proportional to the voltage command. The solenoid valve is connected in series with the resistor, and shares the same variable current input. A flyback diode is also connected in parallel to the solenoid to dissipate kick-back currents when the circuit is turned off.

The actual board design incorporates integrated circuits (ICs) that handle serial communication, digital-to-analog conversion (DAC) and parallelly drive 8 solenoid valves (Figure 3.5). Heatsinks keep the board at operational temperature even at the highest current load (Figure 3.6). This integrated design allows easy fabrication, installation and programming of new olfactometer setups.

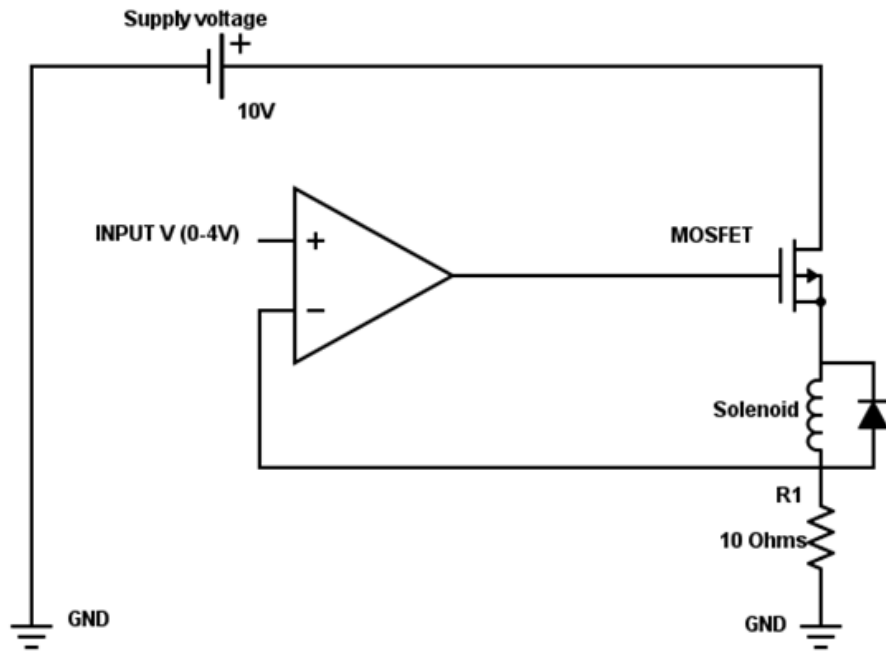


Figure 3.4. Control circuit for EPVs.

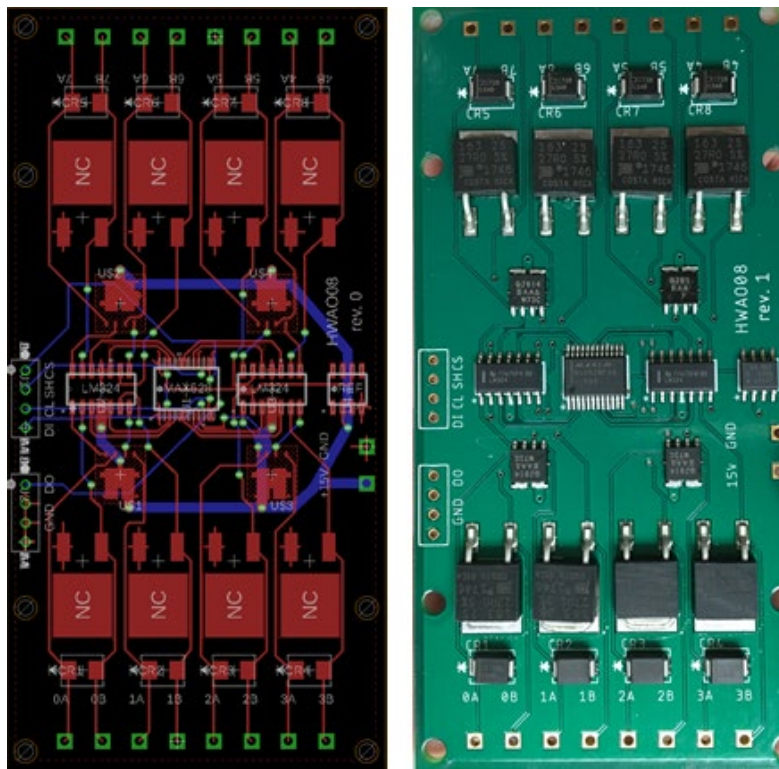


Figure 3.5. Design and finished PCB control circuit for controlling 8 EPVs.

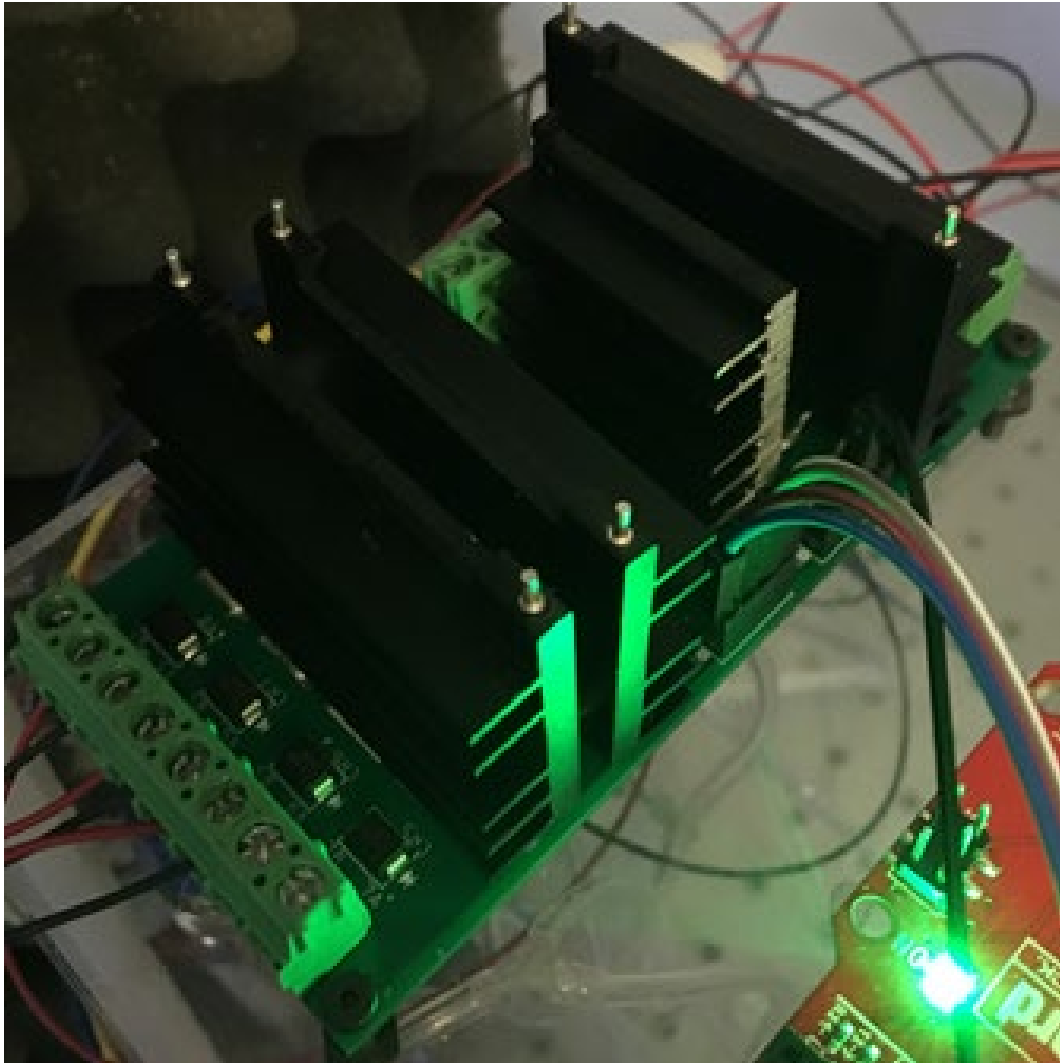


Figure 3.6. Heatsink for the PCB control circuit.

### 3.4 Electronic calibration

Though the flow rate through the EPV varies continuously with the input current, the relationship is not linear. A calibration table is generated, so that control software can linearly vary the flow rate (Figure 3.7).

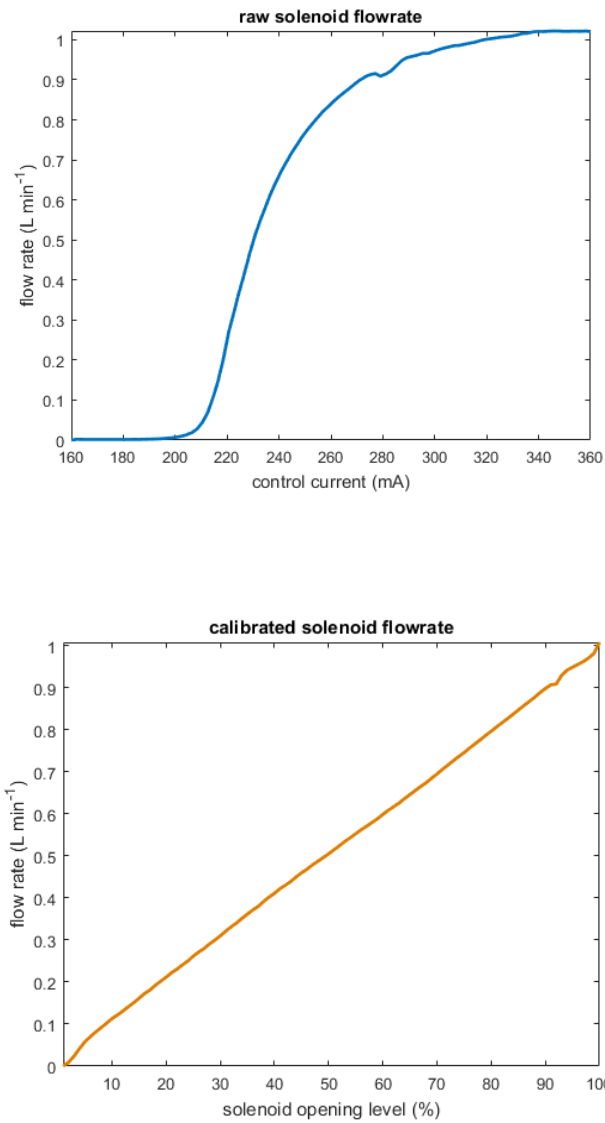


Figure 3.7. top: Flow rate vs. current through EPV bottom: Calibrated flow rate.

### 3.5 Flow balancing and pulse generation

An actual olfactometer incorporates many EPV valves and channels (Figure 3.8). For each channel, air passes through a solenoid valve, a check valve, an odor valve and a second check valve. The check valves prevent odor molecules diffusing out when the solenoid valves are closed, and protects the solenoid valves from odor contamination. Very short tubing combines the different channels immediately before the odor port on the face mask to keep temporal broadening of odor pulses at minimum. One of the vials contains no odor, yielding only clean air in the flow path. The amount of the odor The flow rate of each odor channel can be independently adjusted and complemented by the clean air channel, so that any given time, the flow into the odor port is kept at 1L/min. The concentration of an individual odor at the odor port is then a fraction of the odor vapor pressure in the corresponding odor vial. The fraction is determined by the ratio between the flow rate of the corresponding odor channel and the flow rate at the odor port (1L/min). The flow rate of the face mask exhaust port leading to a vacuum line is equal to the odor port flow rate, so that delivered odor molecules are quickly removed from the face mask. The exhaust stops odor molecules from accumulating in the mask and ensures the off-ramp of an odor pulse is steep.

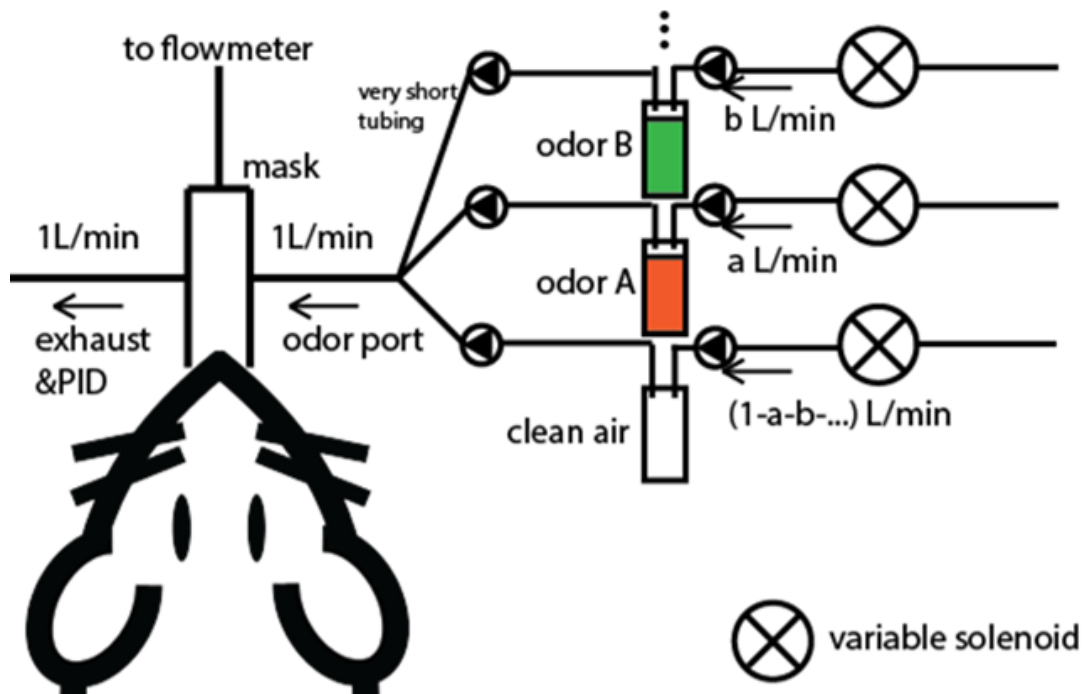


Figure 3.8. Schematic of the fast analog olfactometer.

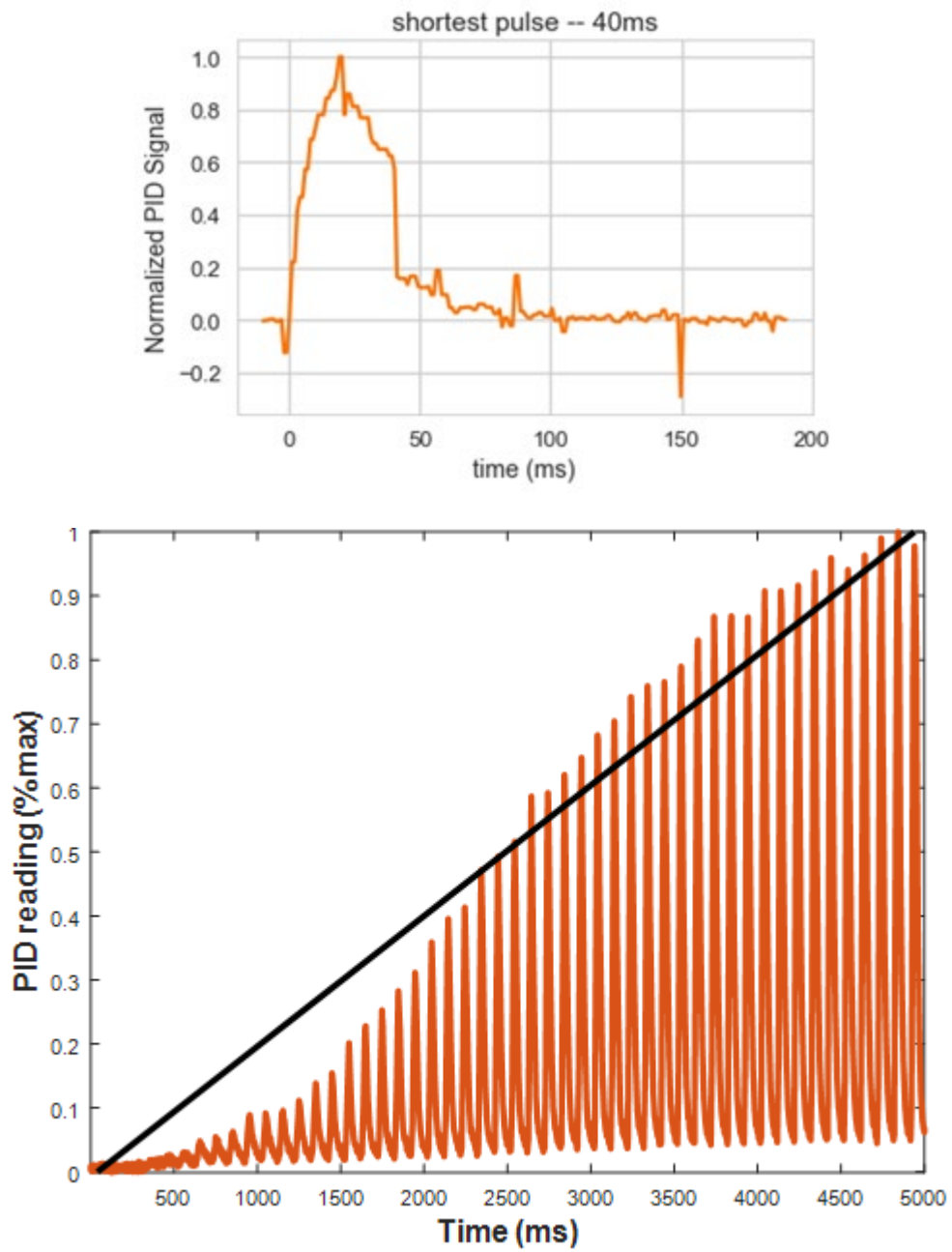


Figure 3.9. top: 40ms odor pulse bottom: 50ms odor pulses delivered at varying concentration.

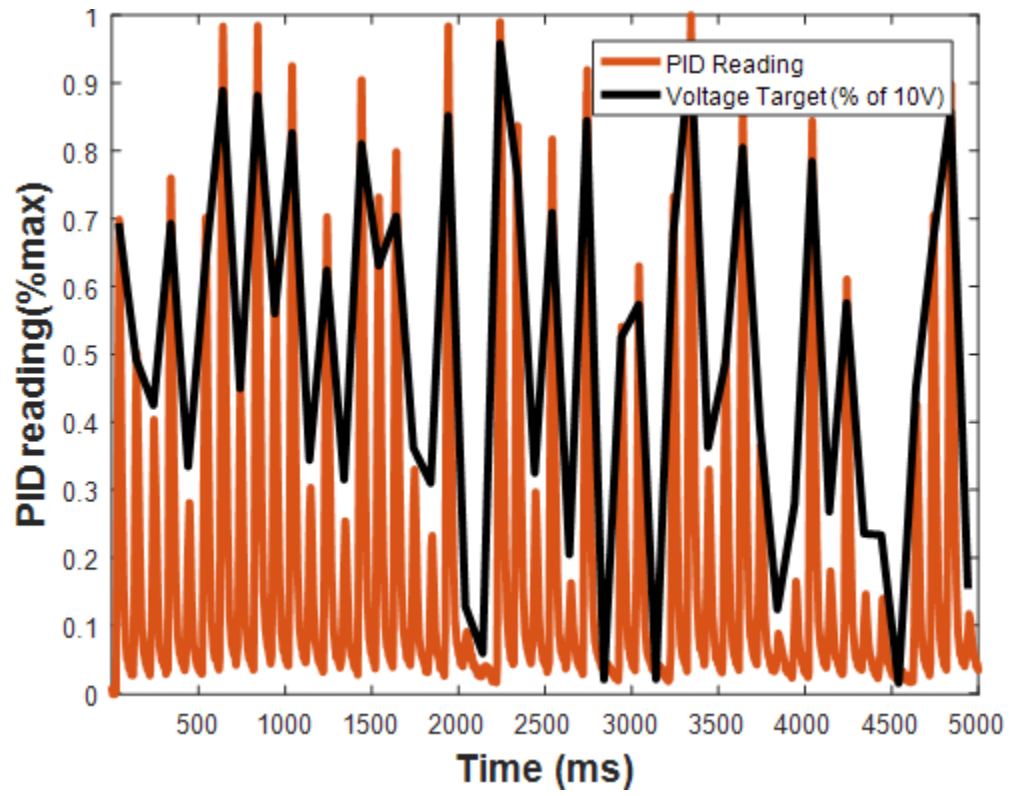


Figure 3.10. 50ms odor pulse delivered at quickly changing odor concentration.



### 3.6 Potential uses of fast analog olfactometer

The fast analog olfactometer is able to deliver short odor pulses with smoothing varying odor levels (Figure 3.9) and can generate rapidly changing odor pulses with 50ms pulse width and concentration ranging from 0.3% to 100% (0.3% steps) of odor vapor concentration in the odor tube. (Figure 3.10) and odor mixtures, and significantly expands the stimuli space of olfactory research. The research result in the following chapters demonstrated the olfactometer's capability in delivering extremely short odor pulses unachievable by previous designs. The short temporal-width of odor stimuli allowed the investigation of mice's neural encoding, perception and behavior response of a series of discrete odor detection events. Furthermore, study of complex odor mixture with temporally non-overlapping individual components and quickly changing composition can be studied.

## 4. Sniffing modulation of olfactory sensory neurons

### activities

#### 4.1 Sniffing and the rate of sniff in head-fixed behavior task

As mentioned in the Chapter 1, mice sample odor cues through sniffing in the air carrying the odor molecules surrounding its nostrils. A unit of sniff starts with the inhalation of air. The inhalation is then followed by exhalation. Only odor molecules arriving during the phase of inhalation enter the nostrils and bind to the olfactory receptors in olfactory sensory neurons. The phase of sniffing can be determined by analyzing the peaks of flow rate from the nostrils of the animal. The flow rate of the animal's nostrils is measured by a flow rate sensor attached to the odor-delivery mask (Figure 3.8).

Freely-behaving mice increase their rate of sniff during odor-guided behavior tasks from a baseline, resting frequency of 2Hz to a higher frequency of 4-12Hz (Wesson et al. 2008). In the head-fixed experiments described in this thesis, the amplitude of sniff remained stable (Figure 4.1) and the frequency of sniff ranged from 3Hz to 10Hz (Figure 4.2)

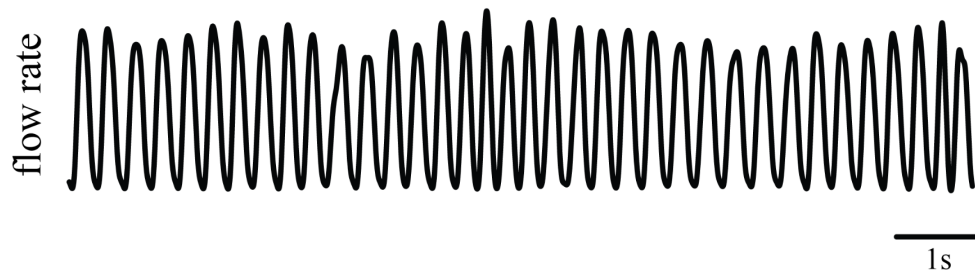


Figure 4.1. the sniffing flow rate of a mouse during a head-fixed behavior task.

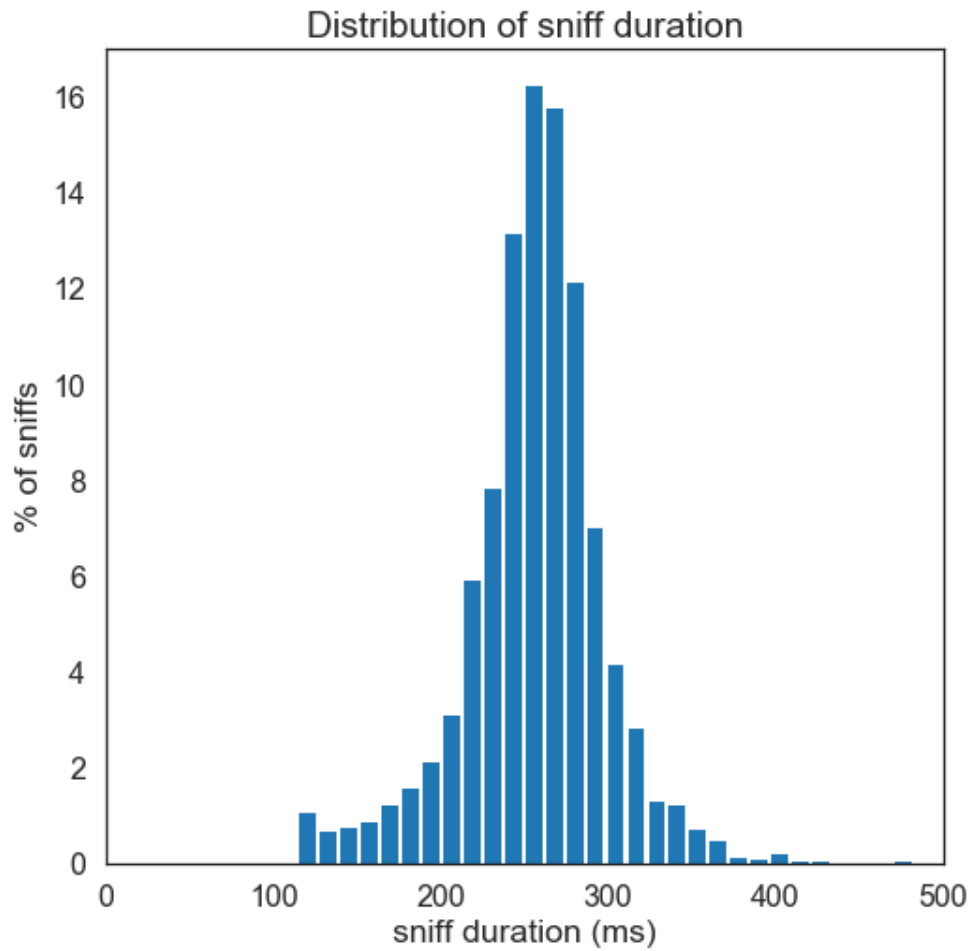


Figure 4.2. Distribution of sniff duration during a head-fixed behavior task.

## 4.2 Sniffing modulation of OSN activities

During experiments, short odor pulses with the sample temporal width and concentration profile were delivered to the nostrils of the animal and calcium imaging was performed on the olfactory bulb glomeruli. Odor pulses arriving at different times elicit different amplitudes of OSN responses. Though the odor pulses shared the same odor identity, temporal width and concentration profile, different amounts of odor molecules could be inhaled in each sniff, yielding differences in OSN responses. To characterize how the sniffing behavior modulates the OSN responses to short odor pulses, calcium imaging of the olfactory bulb glomeruli was performed while head-fixed mice sampled randomly arriving odor pulses from in a facemask. The odor pulses are 50-ms long with the same peak concentration and odor identity (ethyl valerate). ~30 glomeruli in the field of view (FOV) could be identified to show strong response to ethyl valerate (Figure 4.3). Calcium fluorescent traces are extracted from these glomeruli and normalized so that the highest  $dF/F$  equals to 1. The OSN activities elicited by an odor pulse of the sample profile varies dramatically from sniff to sniff (Figure 4.4). Odor pulses with peak concentrations arriving during exhalations elicited much lower OSN activities than odor pulses with peak concentrations arriving during inhalations (Figure 4.5).

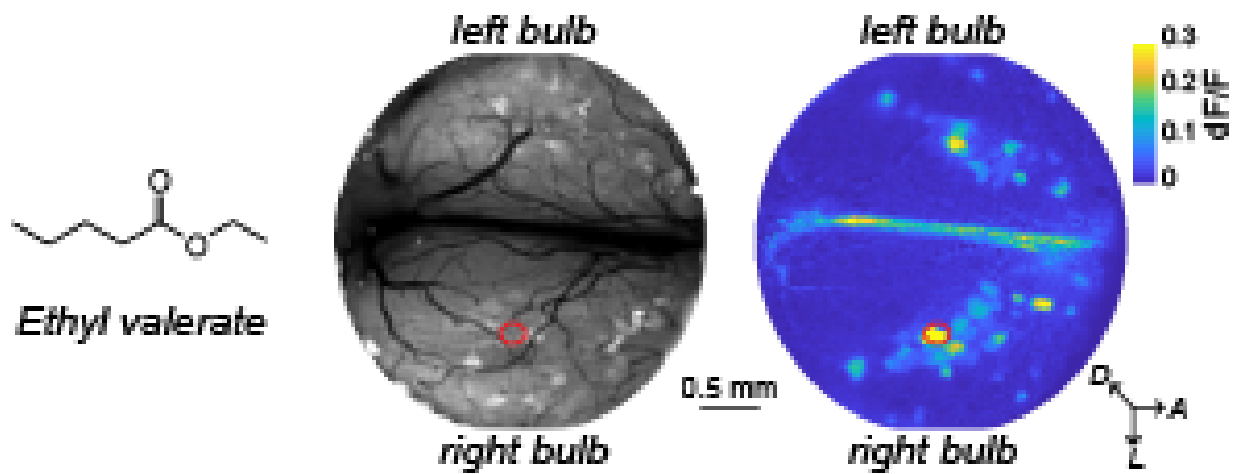


Figure 4.3. left: molecular structure of ethyl valerate. center: calcium fluorescence image of the FOV in OB. right: max dF/F image of the FOV. GCaMP signal shown in Figure 4.4 was extracted from the glomerulus marked by the red circle.

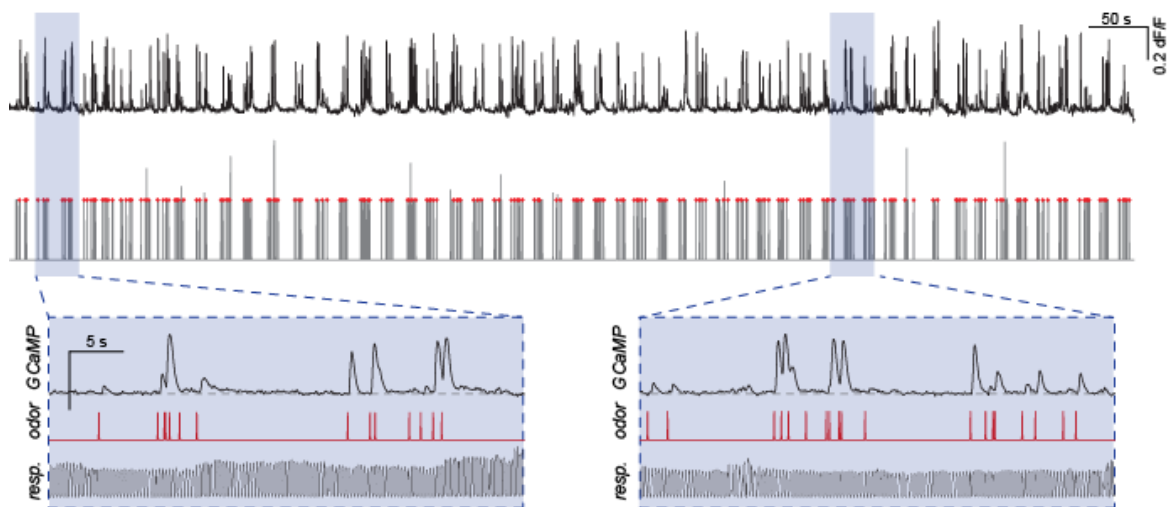


Figure 4.4. top: GCaMP from a selected OB glomerulus. middle: intensities of delivered odor pulses. Bottom: Zoomed-in comparison of GCaMP signal, odor pulse timing and respiration/sniffing flow rate.

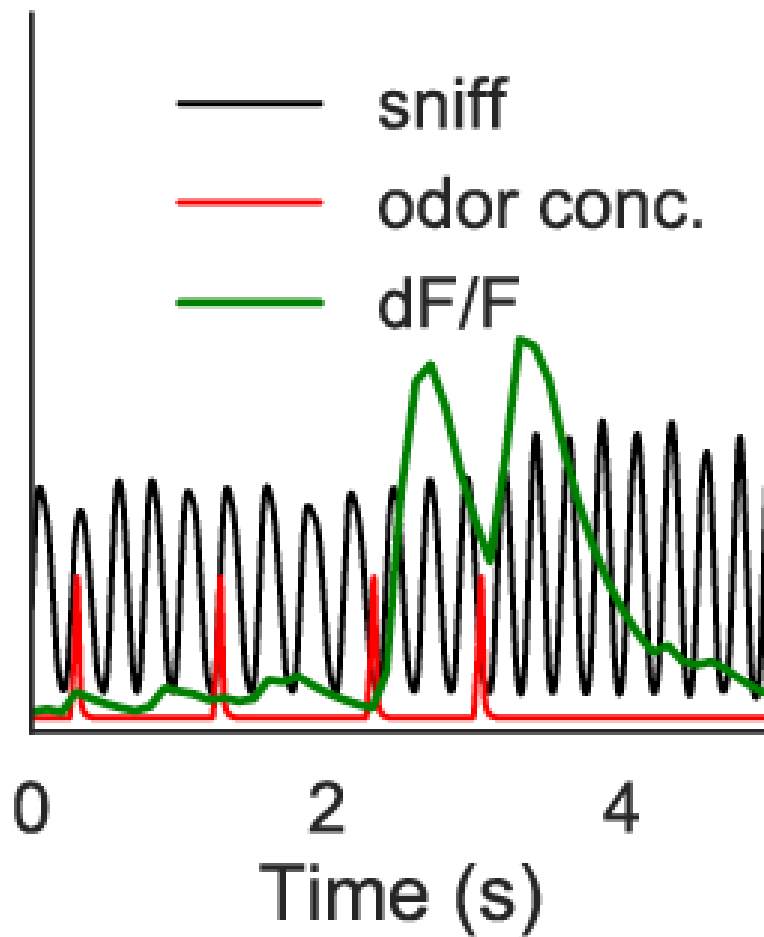


Figure 4.5. Odor pulses arriving during inhalation and exhalation elicited dramatically different OSN responses. red: Odor concentration. black: Sniffing flow rate of the animal. green: GCaMP signal from an OB glomerulus.

### 4.3 Phase response curve of odor pulses

The sniffing modulation of OSN responses to odor pulses can be systematically quantified and represented by a phase response curve. In order to obtain the phase of sniff at each time point for variable durations of sniffs, the timings of peaks in sniffing flow rate are marked, and the duration of time between one peak to the next is linearly assigned a phase of 0 to  $2\pi$ . For each odor pulse, the timing of the odor pulse was converted to a phase measurement. The average OSN response amplitude (measured in GCaMP  $dF/F$ ) for odor pulses arriving at each bin of phase between 0 to  $2\pi$  was calculated (Figure 4.7). The average phase response curve was approximately sinusoidal, indicating that odor pulses that arrived in a specific phase of sniffing, likely the phase with the highest inhalation flow rate, elicited the strongest OSN responses. Interestingly, the lowest value in the phase response curve was still  $\sim 25\%$  of the peak OSN response. A possible cause for this phenomenon is that the 20ms tails of odor pulses (Figure 3.9) arriving after exhalation phases elicited odor responses and were inhaled during the inhalation cycle of the next sniff. The high variance of odor responses for pulses arriving during the exhalation phases were also interesting and requires further analysis in the future.

The OSN activities represent the olfactory sensory input into an animal's brain and could possibly indicate the weight of evidence for each odor pulse. The relationship between the OSN activity and weights of evidence is further investigated in the next chapter.

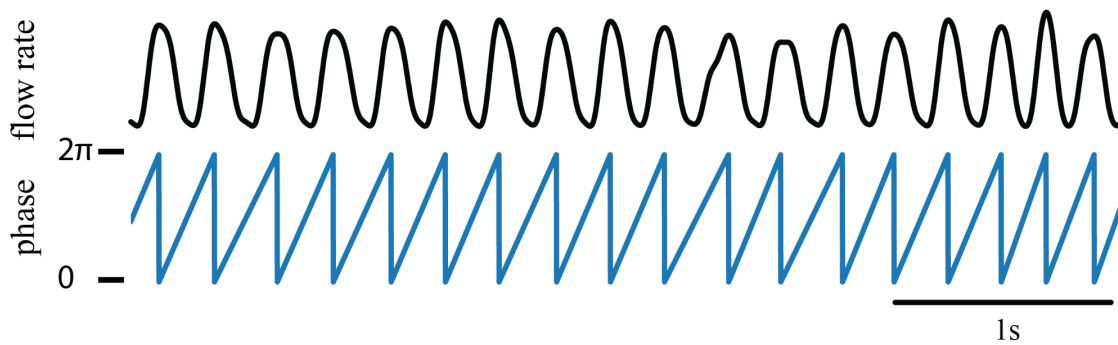


Figure 4.6. top: The sniffing flow rate of a mouse during a head-fixed behavior task. bottom: Phases of sniffing calculated from identifying periods between peaks of flow rate.

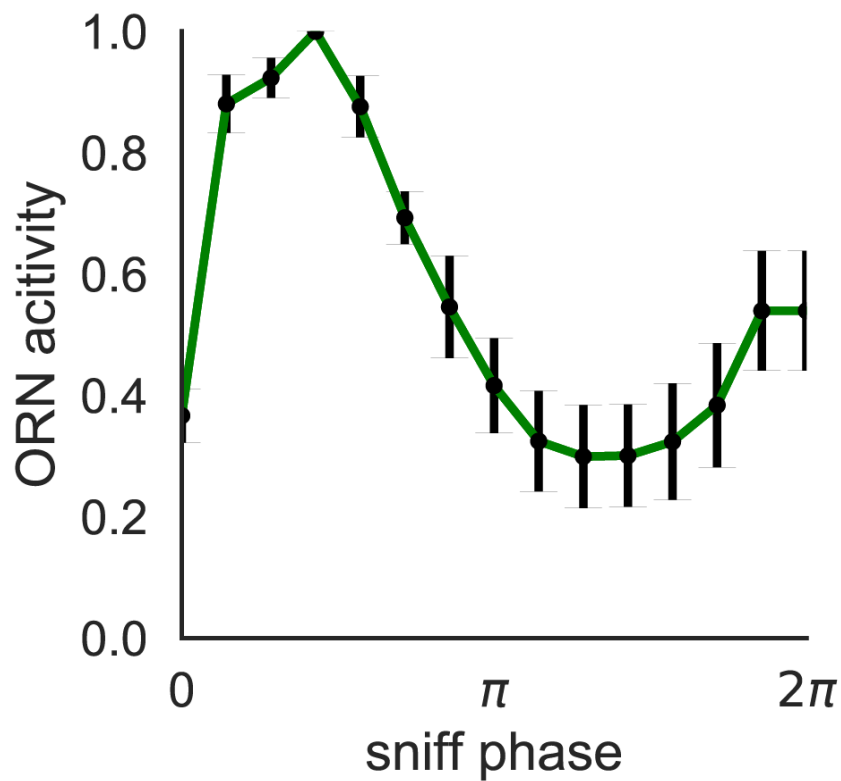


Figure 4.7. Average OSN activity elicited by odor pulses arriving at different phases of sniff. Error bars represent variation between OB glomeruli.



## 5. Olfactory evidence accumulation task

### 5.1 The olfactory evidence accumulation training setup

In order to experimentally study the evidence accumulation of discrete odor pulses, I designed an experimental setup (Figure 5.1) to study olfactory evidence accumulation behaviors in head-fixed mice. The odor stimuli delivered by the fast analog olfactometer. The flow rate in each individual odor line can be varied smoothly between 0 – 1 L/min, and an extra variable line carrying clean air compensated for the change in odor flow and maintained the flow rate at 1 L/min. The percentage of the flow rate of each odor line in the total flow determines the concentration of the odor. The fast analog olfactometer allowed the generation of short odor pulses of 50ms temporal width with arbitrary concentration levels. A specially designed mask is fitted to the nose of the mouse (Figure 5.2), creating a small cavity between the nose of the mouse and the mask. An odor-carrying stream flows into the right side of the mask at a rate of 1 L/min. The left side of the mask is connected to a vacuum line, serving as an exhaust. The flow rate of the odor stream and exhaust is balanced, so that the only net flow into and out of the mask was caused by the breathing and sniffing of the mouse. A flow meter connected to the back of the mask measures the breathing of the mouse.

The ability of the rodents to process airborne cues at diverse distances from the source will be assayed by testing head-fixed mice on a two-alternative forced choice task (2AFC). Two metal lickports (Figure 5.2) were respectively on the left and right side of the animal. To implement a forced time-delay between the onset of the odor stimuli and an animal's decision, the lickports were placed on a linear motorized stage and were only at a distance reachable by the animal at specific times in a task. A foam ball (Figure 5.3) was placed underneath the animal to provide better comfort for the animal and to allow future experiments involving navigation in a virtual reality setting.

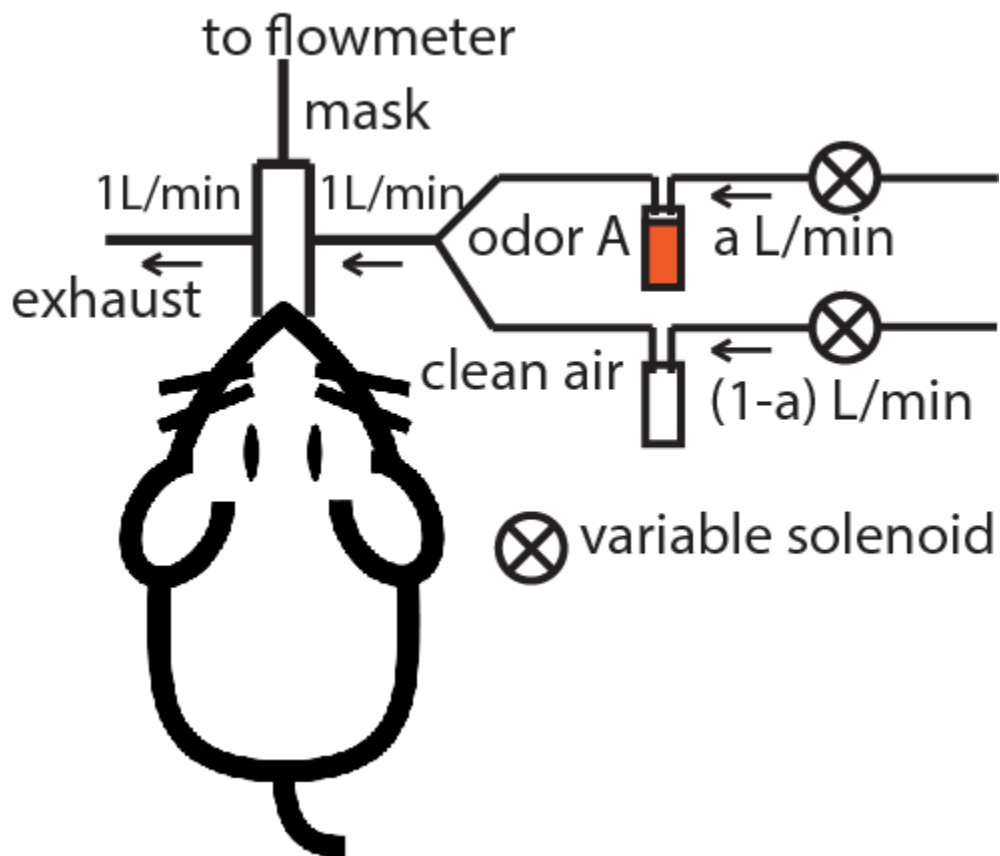


Figure 5.1. The fast olfactometer setup for the olfactory evidence accumulation task.

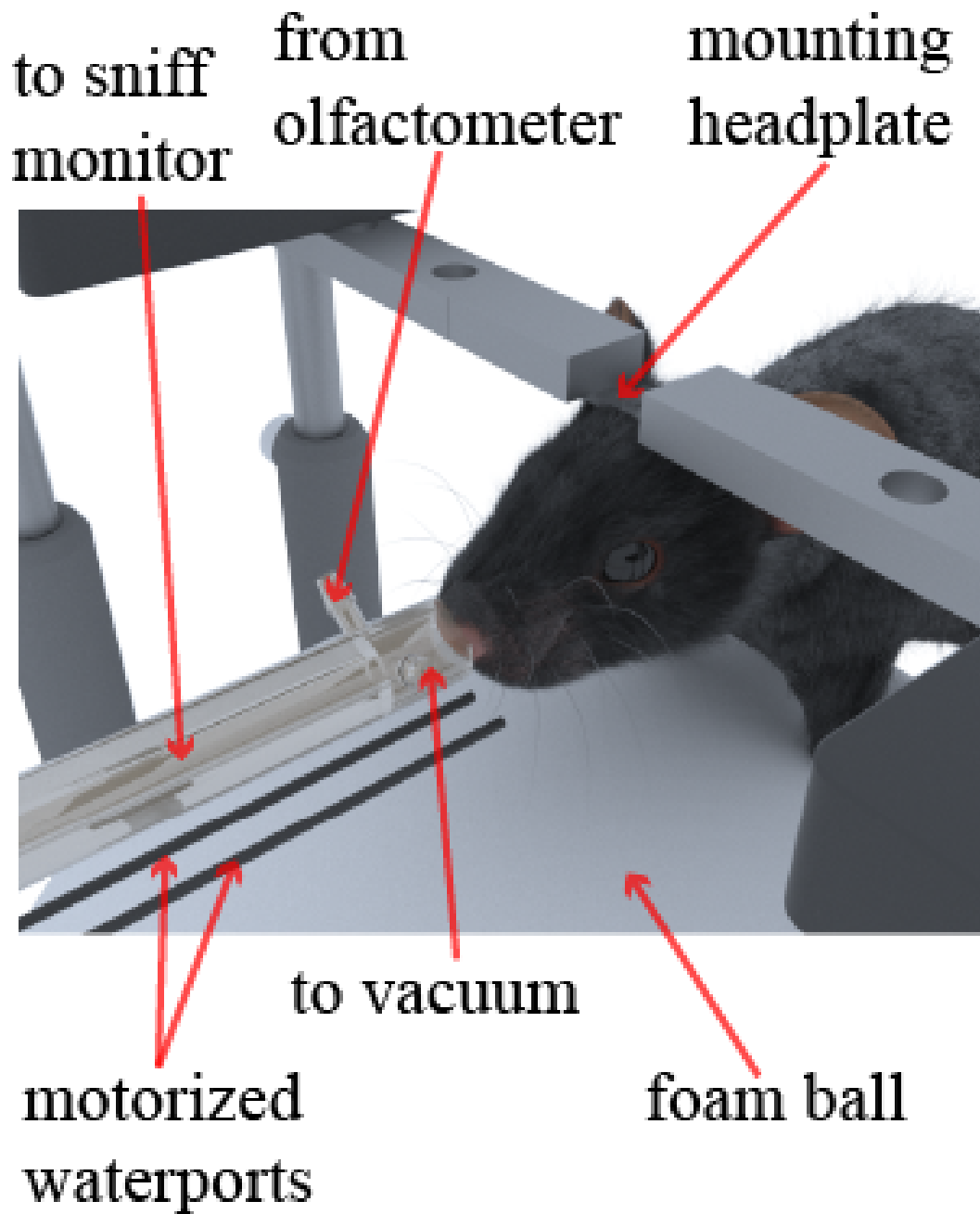


Figure 5.2. Isometric view of the mechanical setup for the evidence accumulation task.

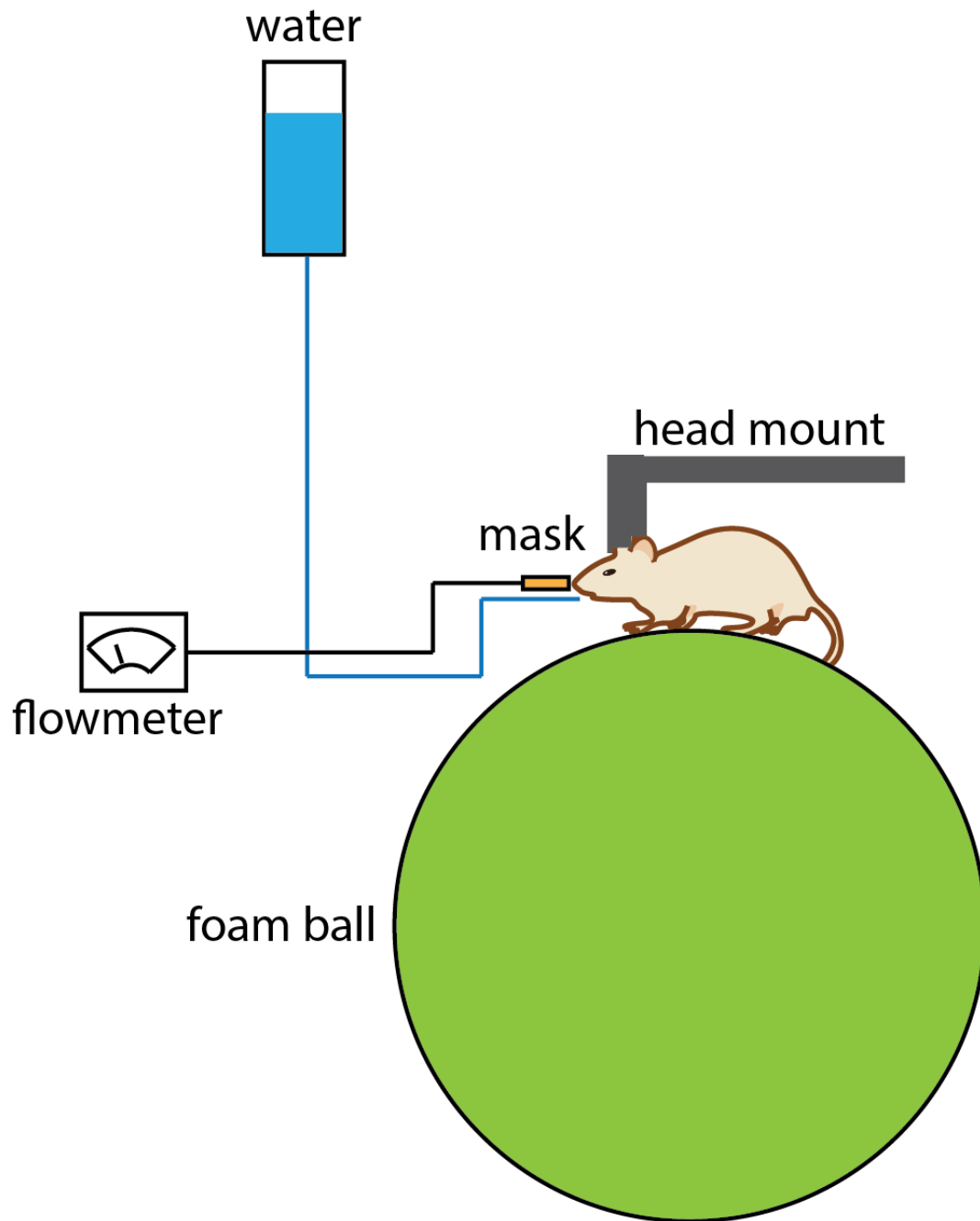


Figure 5.3. Side view of the mechanical setup for the evidence accumulation task.

## 5.2 The olfactory evidence accumulation task

In each olfactory evidence accumulation experiment, a head-fixed mouse was trained to perform in repeated trials where it sampled a few seconds of odor stimuli to then decide between licking left or right to obtain a water reward. In each trial (Fig. 5.4), after an initial wait period, a sound tone marked the beginning of the sampling period. During the sampling period, a number of odor pulses are delivered. After a sound tone marking the end of the sampling period, two water ports moved toward the mouth of the animal (Figure 5.5). The two water ports were respectively associated with high or low number of odor pulses presented during the sampling period. When the mouse licked the correct water port, it was rewarded by a drop of water. When the mouse made a wrong decision, a warning buzz sound was played, and the mouse was put under a 10-second timeout as a punishment before the next trial started.

The duration of the wait period, sampling period and go period can all be tuned, both for animal training purposes and to test different hypotheses. In the following sections, I will discuss the training of animals and the various findings on the evidence accumulation of short odor pulses in mice under different task conditions such as the tasks yielded insights in the influence of integration time and pulse-count contrast on animal performance, evidence weights and decision variability.

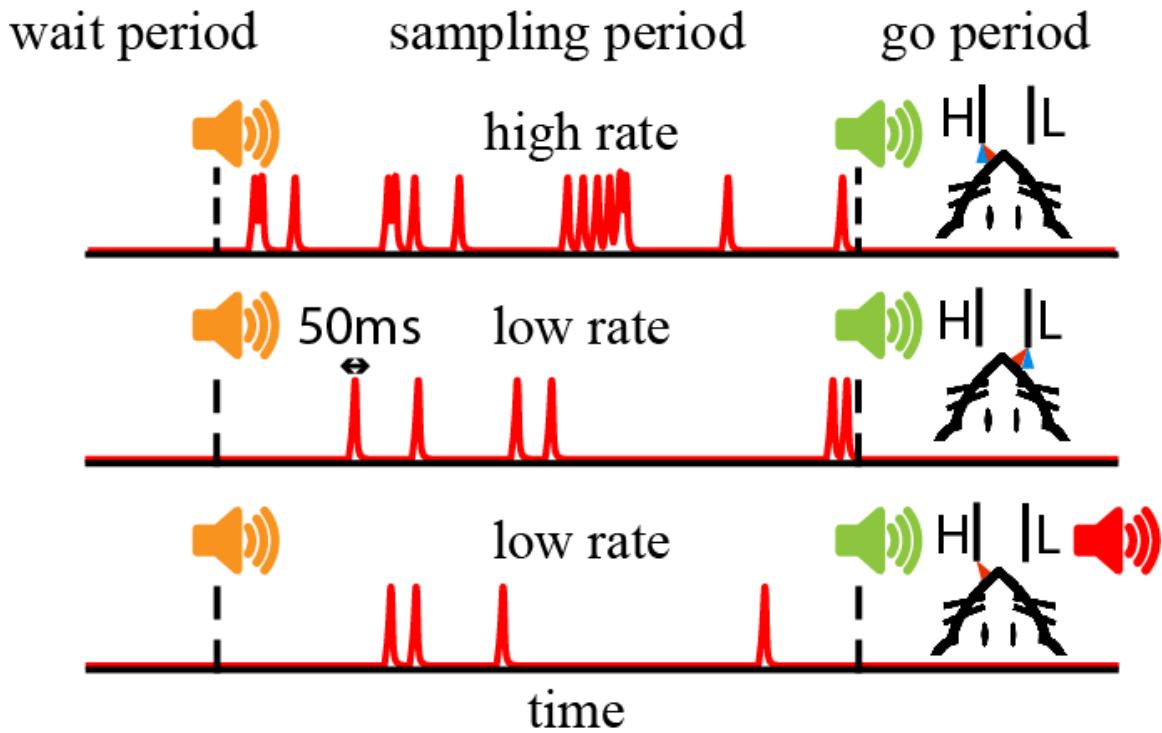


Figure 5.4. Side view of the mechanical setup for the evidence accumulation task.



Figure 5.5. left: Lickport is away from the mouse during wait and sampling period. Right: Lockport is reachable by the mouse during the go period.

### 5.3 The behavior training sequence and animal learning curve

Water restricted mice that were naive to the task were first habituated on the behavior setup for a few sessions with sound tones and moving lickports but no odor stimuli. In these sessions, the animals were rewarded with a few drops whenever the lickports were licked during the go period. By the end of a few sessions without odor stimuli, the animals were accustomed to the task structure and the location of the lickports. Odor stimuli were then introduced, with increasing contrast between high-count and low-count trials and with longer sampling period. Animals learned in one session to differentiate between high contrast counts (10:1) delivered in a short (0.5s) period. When the contrast between pulses was gradually lowered and sampling duration increased session by session, the animal maintained above the criterion performance, where they chose the correct side in over 70% of trials in a session.

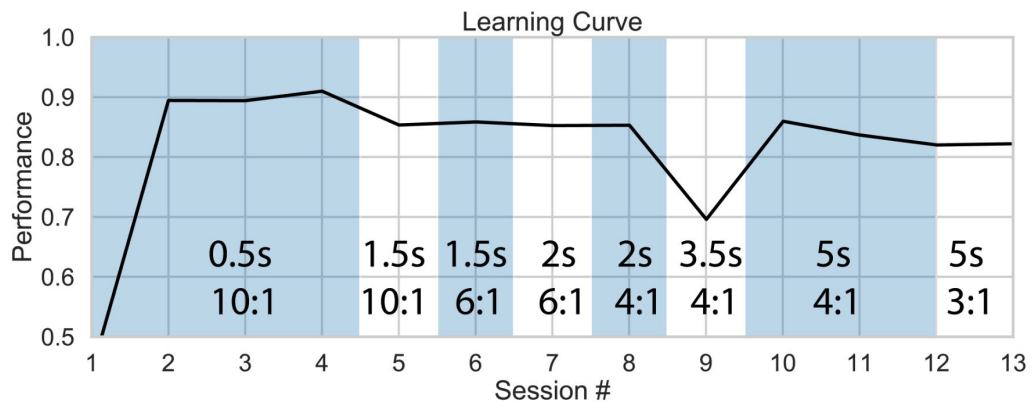


Figure 5.6. Learning curve of a typical animal. Each shaded/light region represent an experimental condition with time and pulse-count contrast indicated in the plot.



## 5.4 Effect of changing sampling time and pulse-count contrast

An animal's performance in an experimental session is defined as the fraction of trials where the animal successfully identified a high or low trial in all the non-idle trials (where animal licked the lickports) in the session. To study the influence of sampling time and contrast of pulse count's on performance, the animals were given a fixed number of pulses in low trials (~ 1 pulse per second) and high trials (~2-6 pulses per second). The timing of each pulse was random and uniformly distributed across the sampling period. In each experimental session, the sampling time and ratio between pulse number of high trials and pulse number of low trials are fixed. The performance increased with sampling time and contrast ratio between the number of pulses in high trials and low trials (Figure 5.7). Animal's performance did not improve when the sampling time increased from 5 seconds to 10 seconds.

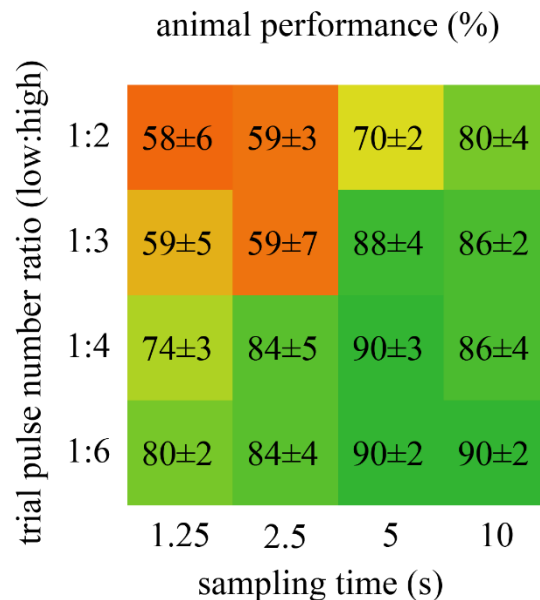


Figure 5.7. Average ( $N_{\text{animal}}=3$ ) session performance of animals in experimental sessions with different sampling time and contrast between high and low pulse count.

## 5.5 Weight of evidence across the sampling period

Pulses arriving at different times during the sampling period can contribute differently to the decision of the animal in a trial. Logistic regression has been implemented in previous research (Deverett et al. 2019) to study the weight of sensory evidence across the sampling period. The sampling period is divided into time bins of 0.5 seconds, and the weight of evidence for odor pulses arriving at each time bin were obtained by a logistic regression analysis where the input is the number of odor pulses in each time bin in a trial, and output is the animal's decision in the trial. For sessions with sampling period from 1.5 seconds to 5 seconds the weights of evidence for different time bins are similar, whereas for sessions with sampling periods of 10 seconds, the weight of evidence was 50% or lower for 1-3 seconds from trial onset. This result suggests that animals weighed the 5-7 seconds most adjacent to their decision making more.

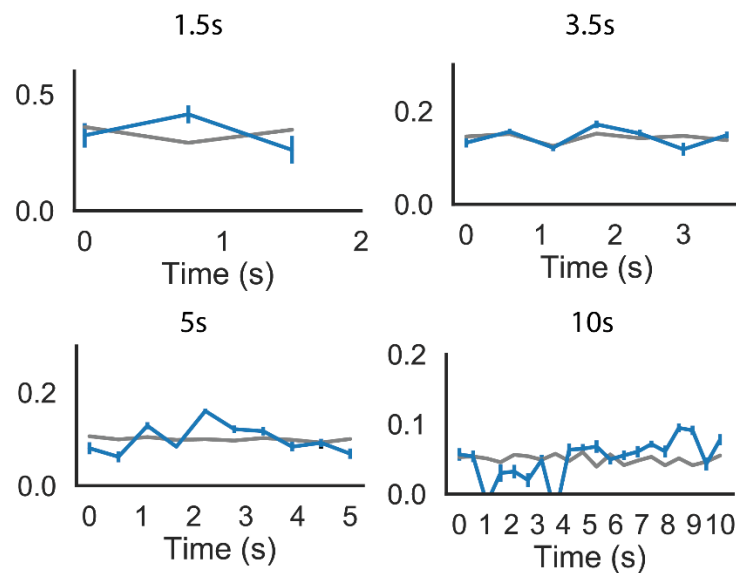


Figure 5.8. Logistic regression weights of evidence in different time bins during the sampling epoch. Blue: weights based on pulse timing. Gray: weights based on shuffled pulse timing.

## 5.6 Task with Poisson-distributed pulse counts

The evidence accumulation task introduced in the previous section implemented fixed pulse counts for high count trials and low count trials. In a turbulent environment in nature, the number of odor detection events in any given time are variable and follows an underlying statistics determined by the wind condition, the landscape and the location of the animal with respect to the odor source. In certain scenarios where the animal is downwind from an odor source, the distribution is Poisson with mean determined by the distance from the odor source. An evidence accumulation task with Poisson-distributed pulse count was introduced to study how mice interpret variable number of odor detection events with underlying statistics. In the tasks described in the following sessions, the sampling period length was 5 seconds and the animals received varying numbers of pulses in each trial. Randomly arriving odor pulses were delivered to the animal's nose at an exponential arrival rate. As a result of the exponential arrival rate, the total number of pulses delivered in the sampling period followed a Poisson distribution (Figure 5.9). Half of the trials were generated using a Poisson process of mean 4, while the other half was generated using a Poisson process of mean 14. Performance approached saturation (~90% correct) when mice differentiated between stimuli with pulse count far from the decision boundary and degraded when rate differences between the binary choices diminished (Figure 5.9). All trained mice reached similar levels of performance.

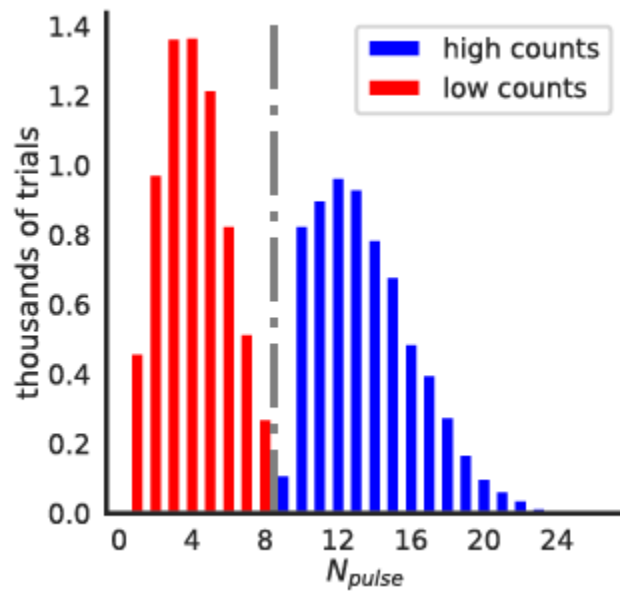


Figure 5.9. Distribution of trials with different numbers of pulses.

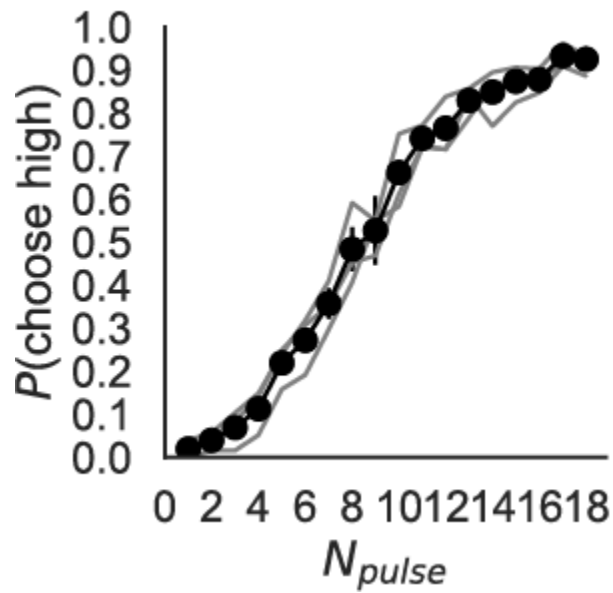


Figure 5.10. Psychometric curves. Gray: individual mice (~4,000 trials per animal) Black: average of all trials across animals (N=3)

## 5.7 Perceptual weights of evidence

As mentioned in Chapter 4, because mice sample odor by sniffing while breathing, the amount of odor molecules inhaled from each pulse will be different if the odor pulse arrives in different phases of sniffing. The OSN activities elicited by odor pulses were modulated by sniffing. This modulation of OSN activities could further lead to differences in the perceptual weights of evidence for odor pulses arriving at different phases of sniff. To study the perceptual weight of evidence, we divided the sniffing cycle into a number of bins and counted the number of odor pulses arriving in each bin in a single trial to generate a phase histogram for that specific trial (Figure 5.10). The phase histogram in each trial was then used as the input to train a logistic regression model to predict the animal's decisions in each trial. The weights of bins of phase of sniff in the logistic regression model after training represent the weights of evidence for different phases of sniff. Logistic regression analysis showed that the perceptual weights of evidence were highly modulated by the phase of the sniffing cycle, and strongly correlated with the sniff modulation of OSN activities (Figure 5.11). Linear regression of OSN activities and perceptual weights of evidence at the same phases of sniff further confirmed the strong correlation (Figure 5.12), suggesting that perceptually mice were accumulating evidence basing on the amplitude of olfactory sensory neuron responses elicited discrete odor pulses.

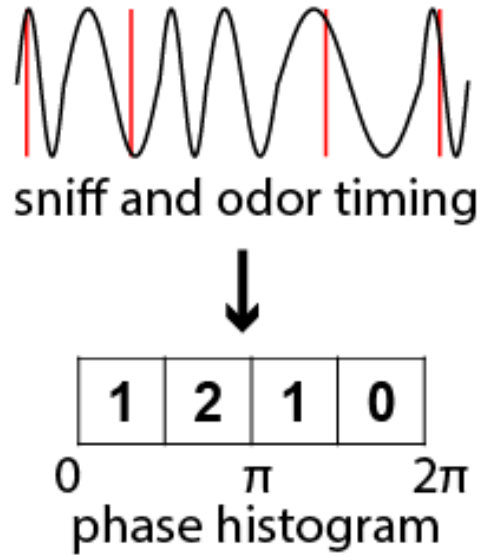


Figure 5.11. Schematic diagram for phase histogram generation.

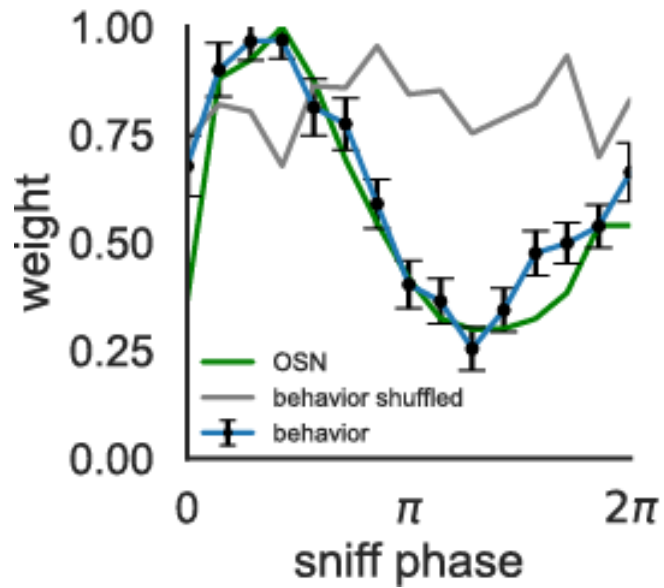


Figure 5.12. Sniff phase weights kernel of animal decision (blue), OSN activity intensity (green), animal decision with shuffled odor pulse timing (gray).

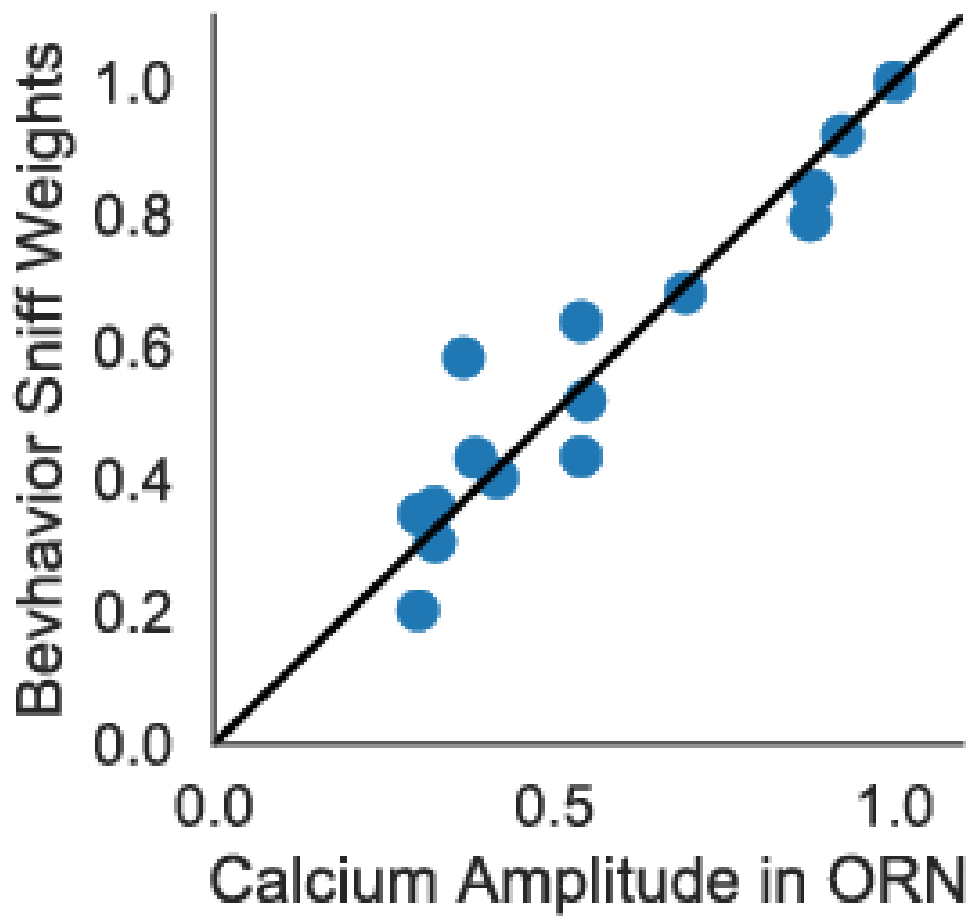


Figure 5.13. Correlation ( $r=0.94$ ) between ORN response and evidence weight of an odor pulse.

## 5.8 Trial history dependency

The choice history of an animal in a behavior experiment can influence the animal's decisions in the subsequent trials (Urai et al. 2019). Combined with the findings in previous section on the weights of evidence, logistic regression models that took phase of sniff and trial history into account predict the animals' decisions in a 10% higher accuracy boundary trials (8 pulses vs 9 pulses), while the accuracies over all trials remain similar above 80% for all models.

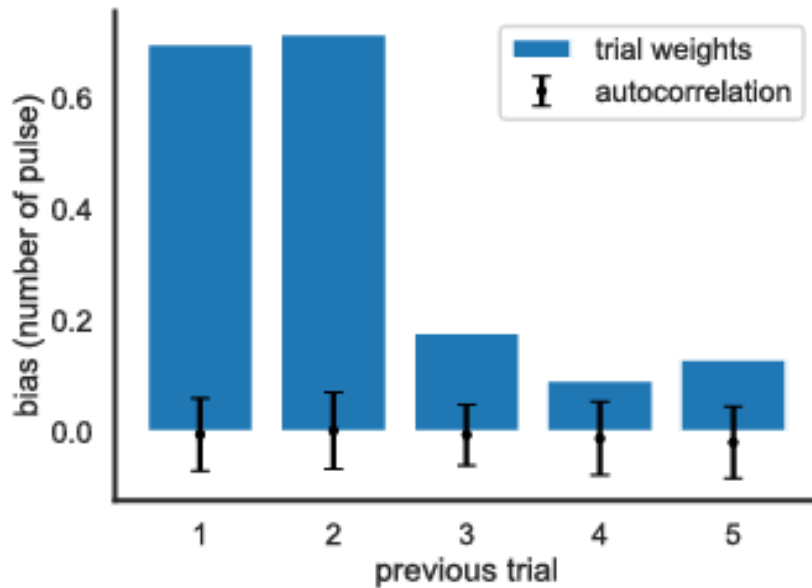


Figure 5.14. Logistic regression weight of decision history. The weight is normalized to the maximum evidence weight in the sniff-evidence weight phase diagram in Figure 5.11.



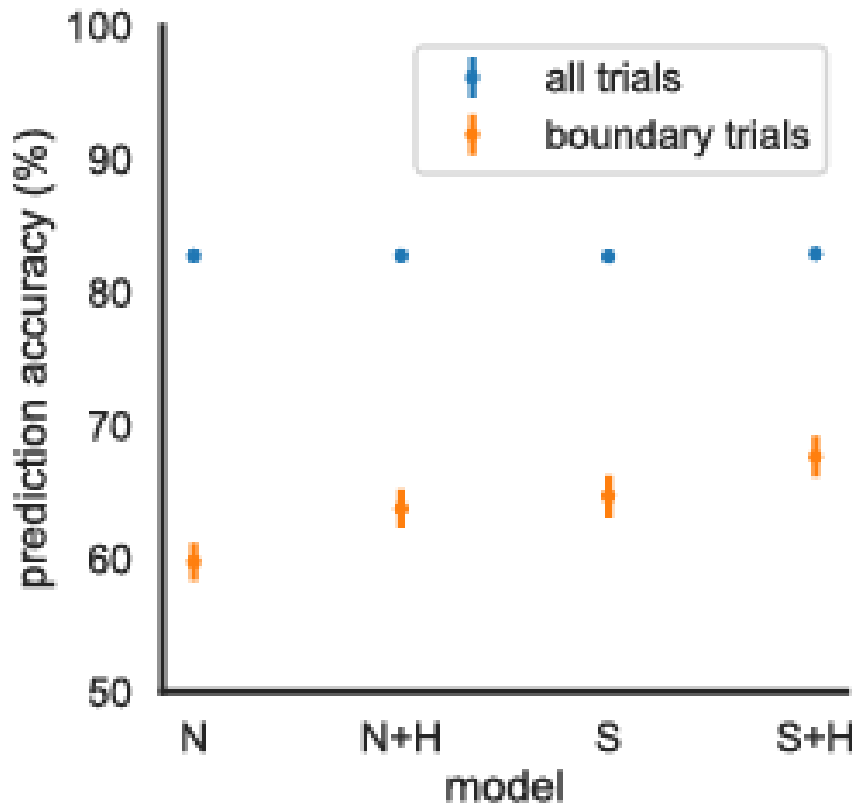


Figure 5.15. Logistic regression accuracy to animals' choices of all trials (blue) and boundary trials (orange, 8 vs. 9 pulses) with different input. N: Total number of pulses only. N+H: Total number of pulses and trial history. S: Sniffing and timing of pulse. S+H: Trial history, sniffing and timing of pulse. For boundary trials, the addition of trial history and pulse timing relative to sniff timing improves regression performance by ~5% respectively.

## 5.9 Sources of variability in olfactory evidence accumulation

Decision making of animals often come with substantial variability, and previous research in behavior modeling of visual and auditory evidence accumulation has been done to characterize the decision variability by modeling different sources of noises in the decision making process (Scott et al. 2015). As shown in Figure 5.9, though mice performed well in the olfactory evidence accumulation tasks and errors still occurred. It is of interest to characterize the variability in the sensory detection and decision making process of animals during olfactory evidence accumulation.

A simple model to characterize the variability in olfactory evidence accumulation is to consider an animal's perception of the number of pulses in a trial as a Gaussian random variable (Figure 5.14). The Gaussian random variable has the mean defined by the actual number of odor pulses delivered to the mask, and the variance specific to the actual number of pulses delivered. In this scenario, two different trials with the same number of odor pulses delivered share the same mean and variance.

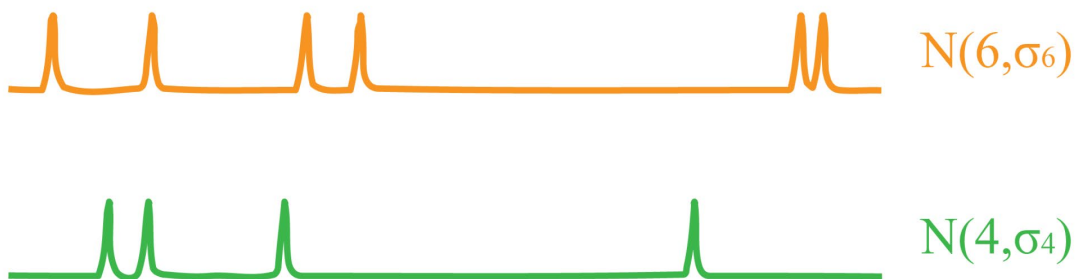


Figure 5.16. Example of a simple gaussian model with trials, trials with different pulse numbers have variability associated with the specific pulse number.

I built a decision model where the animal's perceptual estimation of odor pulse number  $N$  was Gaussian-distributed around the total number of delivered odor pulses in a trial  $N_{\text{pulse}}$  and a variance  $\sigma_N^2$ , where  $\sigma_N^2$  can take different values for different  $N_{\text{pulse}}$  (Fig. 3A). When the difference between the perceptual estimation of odor pulse number and the perceptual decision boundary  $\Delta N$  (Fig. 3B) was greater than zero, the animal would choose high. When  $\Delta N$  was lower than zero, the animal would choose low. The probability of the animal choosing high would be the probability where  $\Delta N$  was positive, defined as the complementary error function of a gaussian at  $\Delta N$  with variance  $\sigma_N^2$ .

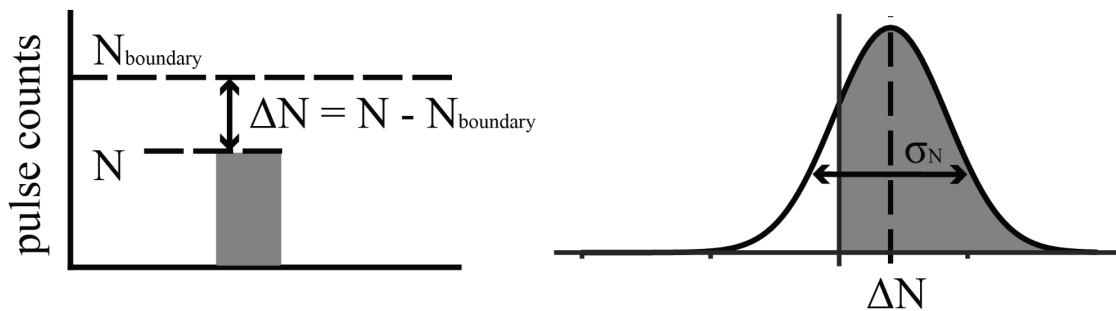


Figure 5.17.  $\Delta N$  is the difference between the number of pulses delivered to the animal and the decision boundary.

Maximum likelihood estimation (MLE) over the entire distribution of  $N_{\text{pulse}}$  showed a linear relationship between  $\sigma_N^2$  and  $N_{\text{pulse}}$  with positive intercept and slope (Figure 5.16), implying a noise associated with pulse-counting and a baseline decision-making noise. A linear-scaling variance model fitted the decision psychometric better than a constant variance model (single variance for all different numbers of pulses), indicated by both the BIC value and the model fit to

animals' psychometric curve (Fig. 5.17). When the sniff modulation of evidence was taken into account, the linear scaling factor of pulse-estimation variability  $k_N$  decreased by ~50% (Figure 5.18) , suggesting a significant portion of variability that was associated with the integration of new evidence was related to the variability in sensory input. The constant term  $\sigma_c$  did not change significantly between the two models, suggesting that there could be variability not associated with sensory noise and variation, but variabilities in the decision-making process.

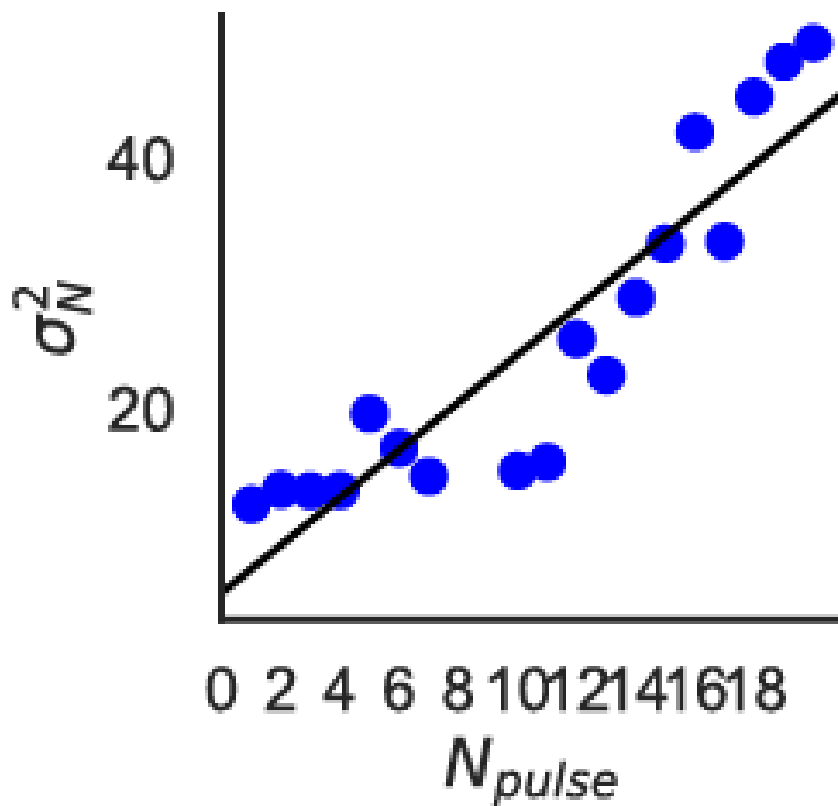


Figure 5.18. Decision-making variances (blue) associated with different numbers of pulses. (R=0.93)

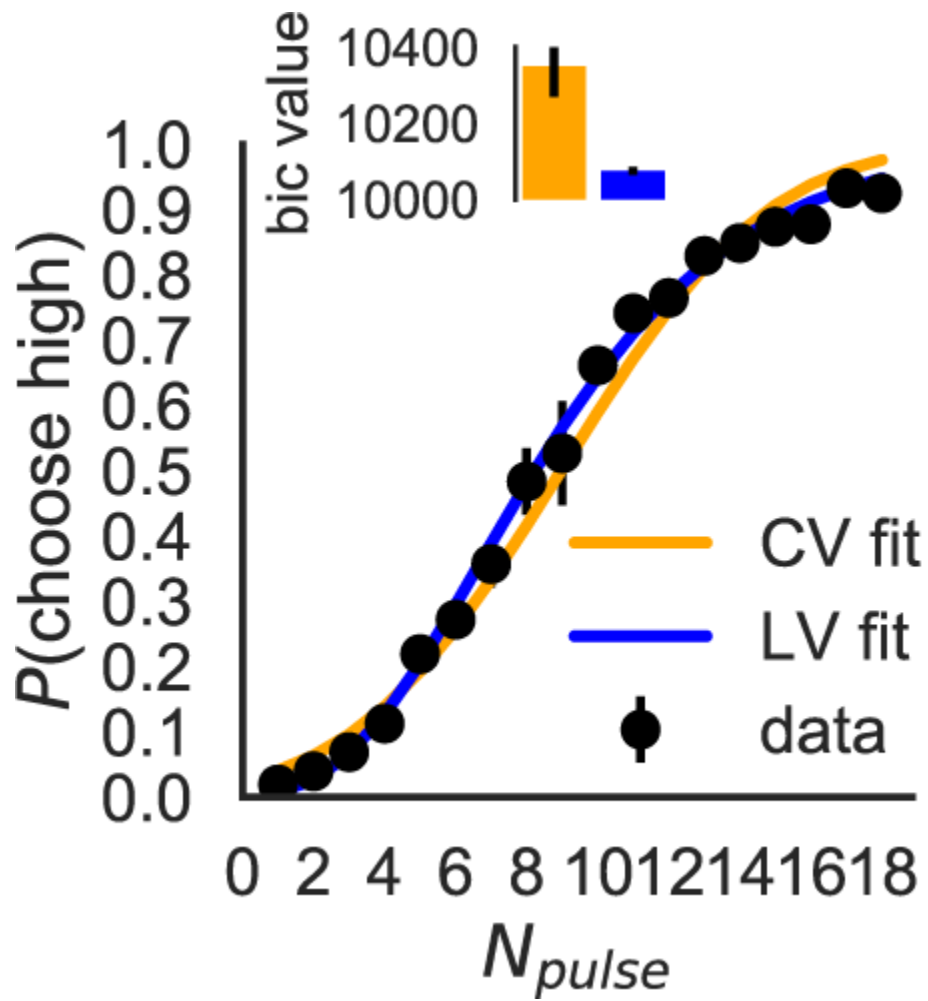


Figure 5.19. Psychometric curve fitting by a constant variance model fit (orange) and a linear scaling variance model fit (blue). Linear variance scaling model fits better to the behavior psychometric.

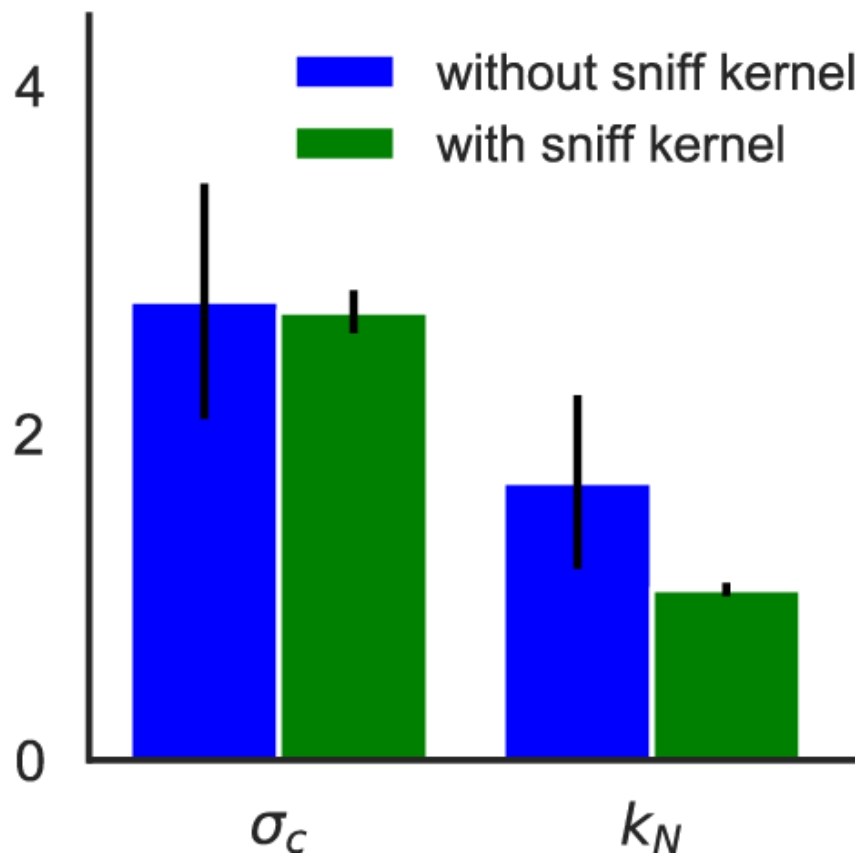


Figure 5.20. Fitting parameters for linear variance scaling model without sniff and pulse timing (blue) and with sniff and pulse timing (green). The baseline variability does not change when sniff and pulse timing is introduced, but the slope of the linear scaling is halved.

## 5.10 Anterior piriform cortex (APC) recording during evidence accumulation

Single-unit neuronal recordings conducted by tetrode drives in the anterior piriform cortex (APC) captured neuronal activities of APC during the olfactory evidence accumulation task with Poisson pulse rate. In each recording session, multiple neurons are found to show activity correlated with the delivery of odor pulses to the animals' noses (Fig. 5.19). Due to the stochastic nature of the stimuli, each trial in the behavioral experiments were different from other trials, making trial-averaging of peri-stimulus neuronal response difficult. To characterize the neuronal response triggered by stochastically arriving pulses, we implemented convolutional dictionary learning (Tolooshams et al, 2020). We were able to obtain response kernels for each neuron to odor pulses, as well as the response intensity to each specific pulses (Figure 5.20). We found that each odor pulse activated a selection of neurons, and the selections of neurons differed from pulse to pulse (Figure 5.21). Overall, a neuron detected ~50% of odor pulses (Figure 5.22), and an odor pulse activated from one to all the neurons for 95% of the pulses (Figure 5.23). These results implied that the activities in APC neurons elicited by short odor pulses were represented in a distributed manner.

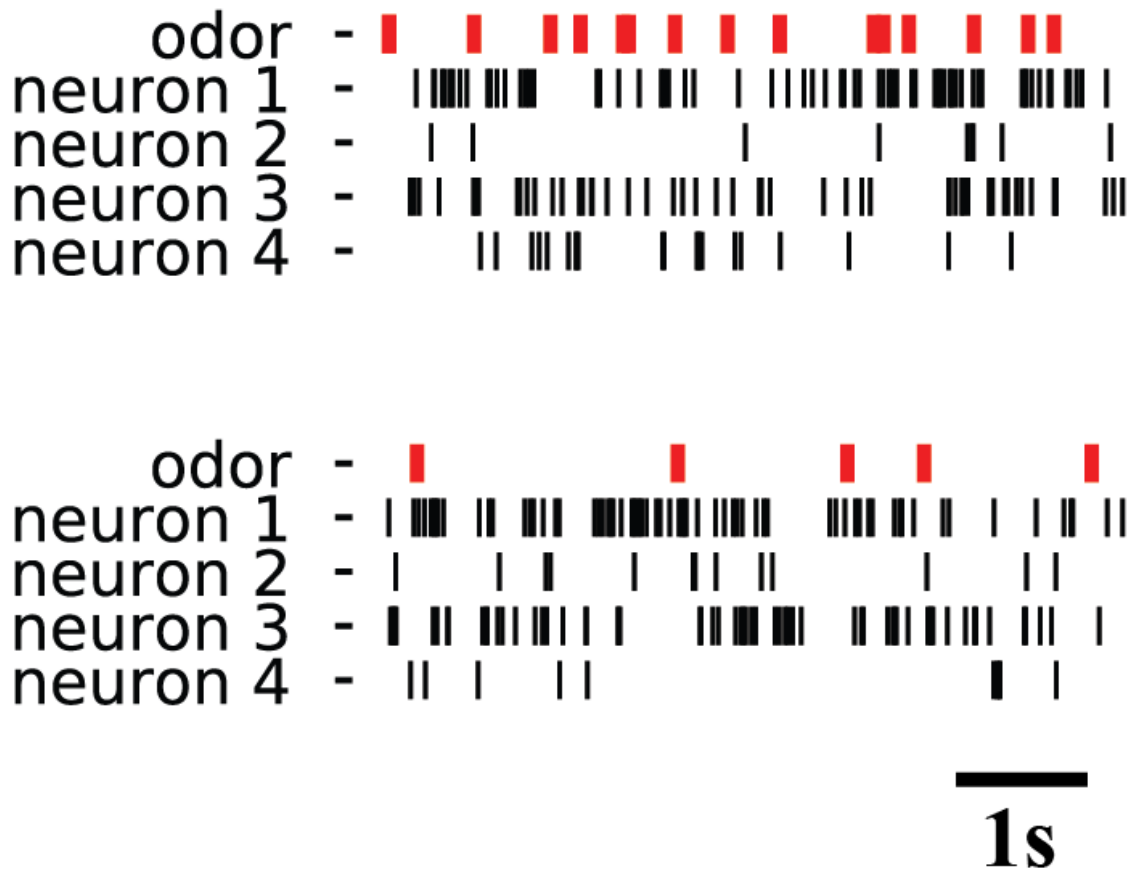


Figure 5.21. Two example trials of recording. Odor pulse (red) and neuronal spiking events of neurons (black) are marked by the vertical line/stripes.



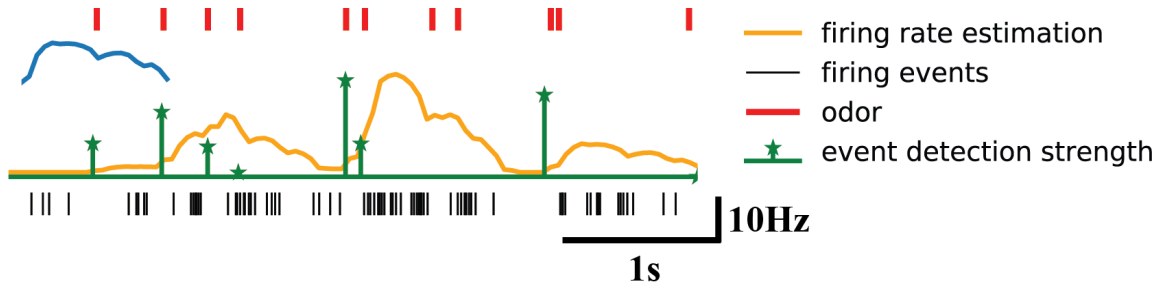


Figure 5.22. Example for neuronal activity extraction in a trial. The neuronal spiking events (black) is represented by a time series of spiking rate (orange) composed of the convolution of an event-based kernel (blue) and events amplitude (green) with timing defined by the odor pulses (red).



Figure 5.23. Example of neurons responding to odor pulses in a trial. Each odor pulse (black strips) triggers a different subset of neurons to respond (colored stripes).

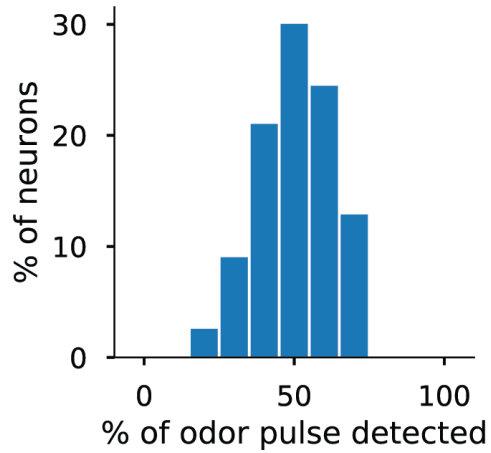


Figure 5.24. Distribution of neurons that respond to a proportion of odor pulses. On average, the neurons respond to half of the odor pulses.

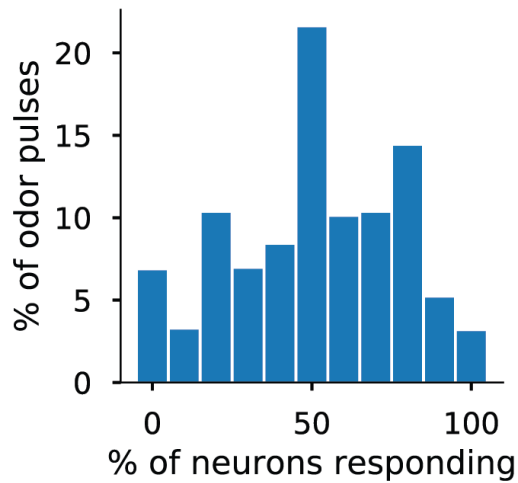


Figure 5.25. Distribution of odor pulses that triggers a proportion of neuronal responses. Most odor pulses trigger at least one recorded neuron to respond.

## 5.11 Sniff modulation of anterior piriform cortex (APC) activities

Previous studies (Bolding and Franks 2017; Bolding and Franks 2018) showed concentration invariant activities in the APC while long odor pulses of concentration levels across several orders of magnitudes were delivered. It is of interest to investigate APCs response for short odor pulses across multiple concentrations, as short pulses of odor could elicit a weaker adaptation in OSNs as well as neurons downstream from the OSNs, leading to potential concentration variant activities. The sniffing modulation of neuronal activities in the APC. K-means clustering of the neuronal phase response of neurons showed that the neurons in APC ranges from sniffing-phase invariant to showing modulation intensity similar to the sniffing modulation in the olfactory glomeruli (Figure 5.24), with most neurons showing lower modulation than that of the olfactory bulb glomeruli (Figure 5.25). The relationship between the sniff phase of odor onset and inhaled odor concentration need to be further studied to determine the concentration dependency of APC activities when short pulses are delivered.

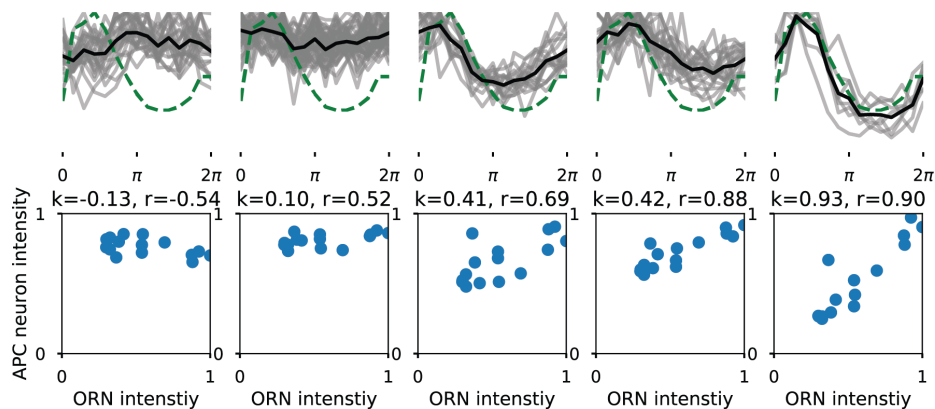


Figure 5.26. Sniff phase response of APC neurons. Some neurons have high correlation with ORN activity and some neurons have low correlation with ORN activity.

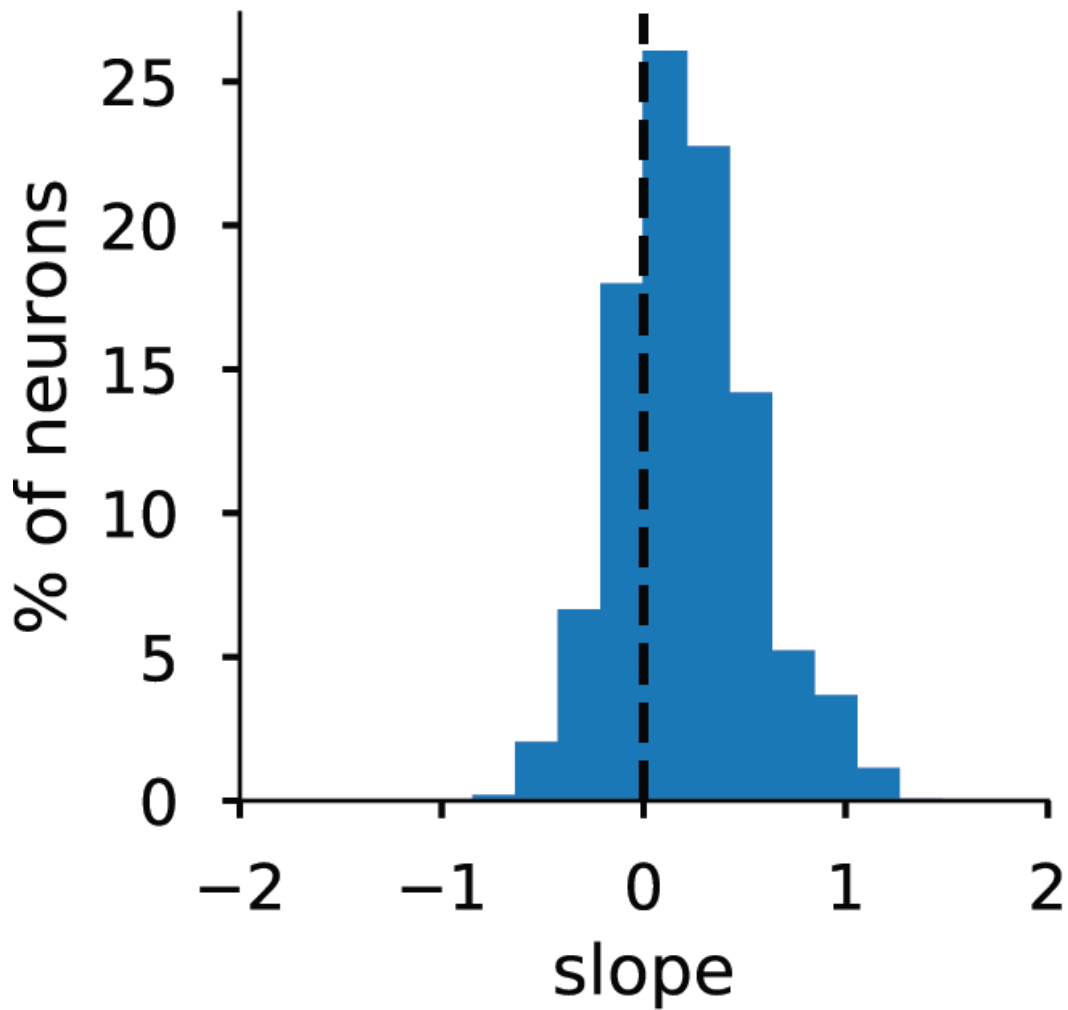


Figure 5.27. The distribution of APC neurons' responses to the odor pulse shows that most neurons have a small correlation with the OSN activity, with a small percentage of neurons having activity that highly correlate with the OSN activity.

## 5.12 Anterior piriform cortex (APC) neural activities represent transient odor information

Multiple linear regression shows that the populational total spike counts of neurons in a trial was strongly correlated with the pulses of neurons when more than 10 neurons were recorded and reached saturation for over 20 neurons (Figure 5.26). Logistic regression of the neuronal activity could be trained to predict the animal's decisions well (Figure 5.27). When neuronal activities over a shorted timespan were included in the regressions, the accuracy drops (Figure 5.28), implying that the activities of APC neurons reflected the transient detection of odor pulses but not the accumulated evidence.

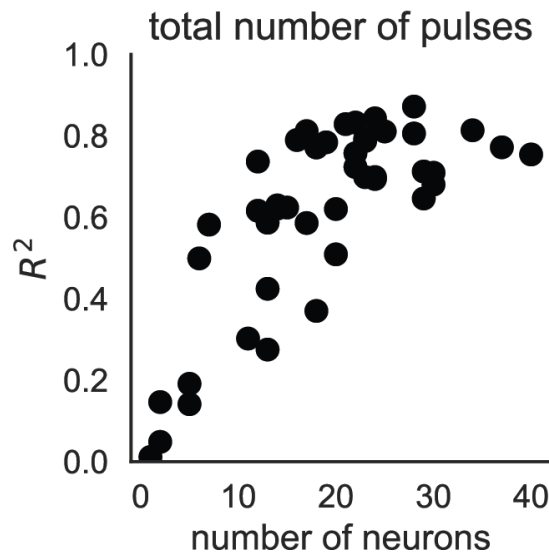


Figure 5.28.  $R^2$  score of multiple linear regression between the total spike counts of recorded neurons in a trial and the total number of pulses in a trial for different sessions.  $R^2$  increases with the number of neurons recorded in a session, getting above 0.6 for more than 10 neurons and saturates at  $R^2=0.8$ .

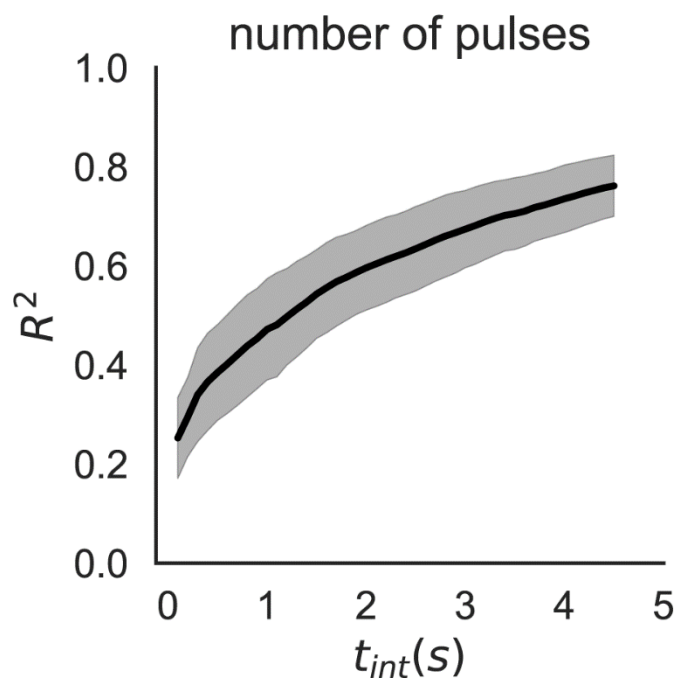


Figure 5.29. Average multiple linear regression  $R^2$  using spike counts of varying time  $t_{int}$  before decision in a trial.  $R^2$  increases with  $t_{int}$ .

## 5.13 Summary of results

The olfactory evidence accumulation task and related recording has shown that mice have the capability to accumulate evidence from discrete, short odor pulses arriving randomly in several seconds. With sampling time under 5 seconds, the weight of evidence of each odor pulse does not depend strongly on the timing of the pulse within the sampling period but depends strongly on the phase of sniff when the pulse arrives at the animal's nostrils. Variability in a mouse's estimation of number of pulses during the accumulation task increases with the number of pulses delivered in the task. A substantial portion of the scaling variability can be attributed to variations in sensory inputs caused by variations in the phases of sniff that odor pulses arrive at. Tetrode recordings in the APC showed no significant representation of a decision variable (DV) associated with the accumulated evidence over time. APC activities were shown to better reflect the transient arrival of odor pulses. APC neuronal activities were found to exhibit varying degrees of dependency on the OSN activities, ranging from invariant to fully correlated to OSN activities.

## 6. Conclusions and Discussions

With the results presented in previous chapters, I have presented a new method to precisely deliver quickly changing odor stimuli, characterized the sniffing modulation of OSN responses to short odor pulses, and shown that mice can perform in evidence accumulation tasks when the sensory stimuli consist of discrete short pulses of odor. I have further shown that the neural representations of the olfactory stimuli during olfactory evidence accumulation task in OB and APC were mainly sensory, representing the detection of transient odor pulses but not the accumulated evidence. The olfactory evidence accumulation task provides ground to more controlled study of olfaction-based navigation in rodents. Furthermore, our platform introduces a new paradigm in perceptual decision-making in which we can, unlike in vision or audition, record neural activity at all levels, from the first layer of sensory neurons to the decision-making networks. The following sections discuss some of the potential implications from these results and further experiments to address these implications.

### 6.1 What is the relationship between the odor concentration and sniffing modulation of OSN response to short odor pulses?

As discussed in early chapters, a strong contributor to the sniffing modulation of OSN responses when short pulses are delivered could be the variation in the amount of odor molecules inhaled by the animal. OSNs are known to show varying degree of activation by different concentration levels of long odor pulses across multiple orders of magnitudes (Lansky and Rospars



1998; Tan et al. 2011). In the experiments described in the study, the odor pulses delivered shares the same concentration profile, and the exact amount of odor molecules inhaled in each sniff was not known. In order to identify the relationship between odor concentration and sniffing modulation of OSN activity. I plan to first create an experimental setup where odor pulses were delivered to suction port with variable flow mimicking the sniff of an animal. A PID detector will detect the odor concentration “inhaled” by the suction port in each artificial sniff to quantify the concentration of odor sniffed by a mouse. This experiment will create a map between the phase response curve in Chapter 4 and odor concentration. Calcium imaging on the OB glomeruli can then be performed on mice when short pulses of different odor concentration levels are delivered at the same phase of sniff and generated an odor concentration response curve. Comparison of the phase response curve, the odor concentration curve and the map between phase response and odor concentration will be able to depict the full relationship between sniffing modulation and concentration dependence in OSN activities.

## 6.2 Are APC neurons concentration-invariant or concentration-variant?

Previous studies (Bolding and Franks, 2017; Bolding and Franks 2018) have found concentration-invariant neurons in APC that maintains the same activity levels when triggered by long odor pulses with concentration levels across different orders of magnitudes. I have found when short odor pulses were delivered, activities of APC neurons showed a range of dependency on the activity of OSNs. While some neurons in the APCs can be described as concentration-invariant, a large portion of APC neurons recorded were modulated by sniff phase and show high

correlation with the OSN activities. Furthermore, the perceptual weight of evidence strongly correlated with the OSN activities, showing that the variation in the input strength of sensory stimuli (e.g. concentration) was kept in the information stream from sensory input to decision making. This suggests that apart from concentration-normalization that were previously observed, input variation such as change in odor concentration still are represented at multiple processing level in the brain.

### 6.3 Where is the decision variable (DV) for olfactory evidence accumulation?

Multiple brain region such as the anterior dorsal striatum (Yartsev et al. 2018), posterior parietal cortex (Akrami et al. 2018), frontal cortex (Scott et al. 2017; Hanks et al. 2015) and cerebellum (Deverett et al. 2019) were found to represent DV or accumulated evidence in visual, auditory and tactile evidence accumulations tasks. Unlike the other senses, the olfactory system has no direct input into the thalamus (Courtiol and Wilson 2015) and could potentially utilize different pathways to compute and represent the DV. In my study, DV was not present in the APC during evidence accumulation task. To investigate whether a DV for olfactory evidence accumulation exists, and to locate the brain region that would represent the DV, I plan to study the neural activities in brain regions downstream to the piriform cortex during the evidence accumulation tasks. The lateral entorhinal cortex (IENT) and the olfactory tubercle (OT) (Diodato et al. 2016) and the orbitofrontal cortex (OFC) (Chen et. al 2014) receive input from the piriform cortex. The odor-value coding in OT (Millman and Murthy 2020) suggests that OT could be a

possible candidate for coding cumulative odor signals that would lead to different rewards. The IENT was known to encode time (Tsao et al. 2018) and was involved in representing egocentric bearing during navigation (Wang et al. 2018). The frequency of odor detection events represents a egocentric distance to an external odor source, and could potentially be represented in the IENT. The OFC's role in decision making (Bechara et al. 2000) and the encoding of values such as confidence (Masset et al. 2020) and reward value (Wallis 2007) makes the brain region a potential place to process DV in evidence accumulation tasks. Additionally, The post piriform cortex (PPC), which hasn't been studied in this work, could also be a potential brain region where representation of the decision variable can be found.

## 6.4 Is the accumulated evidence utilized in olfaction-based navigation?

Virtual reality (VR) experiments (Minderer and Harvey 2016) have shown success in studying mouse navigation using visual (Harvey et al. 2009; Morcos and Harvey 2016; Runyan et al. 2017) and continuous odor signals (Radvansky and Dombeck 2018). However, the way animal navigates through a turbulent odor landscape still remains to be studied. My study has shown that mice indeed have the capability to integrate discrete odor pulses and make decision based on turbulent odor stimuli. I plan to integrate the olfactory evidence accumulation behavior with virtual reality and create a navigation task, where animal navigate through a virtual landscape based on turbulent odor whose detection frequency is dependent on the animal's distance to the "odor" source in the virtual space.

## Bibliography

- Albeanu, D., Provost, A., Agarwal, P., Soucy, E., Zak, J., & Murthy, V. (2018). Olfactory marker protein (OMP) regulates formation and refinement of the olfactory glomerular map. *Nature Communications*, 5073.
- Angyán, & Szirmai. (1967). Recording of respiration with thermocouple in freely moving cats. *Acta physiologica Academiae Scientiarum Hungaricae*, 31(1), 73–6.
- Bechara, A., Damasio, H., & Damasio, A. (2000). Emotion, Decision Making and the Orbitofrontal Cortex. *Cerebral Cortex*, 295–307.
- Bolding, K., & Franks, K. (2017). Complementary codes for odor identity and intensity in olfactory cortex. *eLife*, 6, e22630.
- Bolding, K., & Franks, K. (2018). Recurrent cortical circuits implement concentration-invariant odor coding. *Science*, 361(6407), eaat6904.
- Brody, C., & Hanks, T. (2016). Neural underpinnings of the evidence accumulator. *Current Opinion in Neurobiology*, 37, 149–157.
- Brunton, B. W. (2012) *Optimal accumulation of evidence for decision-making in rats* [Doctoral dissertation, Princeton University]
- Brunton, B., Botvinick, M., & Brody, C. (2013). Rats and Humans Can Optimally Accumulate Evidence for Decision-Making. *Science*, 340(6128), 95–8.

- Buck, L., & Axel, R. (1991). A novel multigene family may encode odorant receptors: A molecular basis for odor recognition. *Cell*, 65(1), 175–187.
- Celani, A., Villermaux, E., & Vergassola, M. (2014). Odor Landscapes in Turbulent Environments. *Physical Review X*, 4(4), 041015.
- Chang, E., Frattini, S., Robbiati, S., & Huerta, P. (2013). Construction of Microdrive Arrays for Chronic Neural Recordings in Awake Behaving Mice. *Journal of Visualized Experiments*, e50470.
- Chen, C.-F., Zou, D.-J., Altomare, C., Xu, L., Greer, C., & Firestein, S. (2014). Nonsensory target-dependent organization of piriform cortex. *Proceedings of the National Academy of Sciences*, 16931–16936.
- Chen, T.-W., Wardill, T., Sun, Y., Pulver, S., Renninger, S., Baohan, A., ... Kim, D. (2013). Ultrasensitive fluorescent proteins for imaging neuronal activity. *Nature*, 295–300.
- Clarke, Panksepp, Trowill, & Pankseep. (1970). A method of recording sniffing in the free-moving rat. *Physiology & Behavior*, 5(1), 125–126.
- Connell, J. (1966). An instrument for measuring the effective cross-sectional nasal airway. *Journal of Allergy*, 37(3), 127–134.
- Courtiol, E., & Wilson, D. (2015). The olfactory thalamus: unanswered questions about the role of the mediodorsal thalamic nucleus in olfaction. *Frontiers in Neural Circuits*, 9, 49.

- Crossland, Horsfall, Oxenham, Shaw, & Turnbull. (1977). A simple device for measurement of respiratory rate in the mouse [proceedings]. *British journal of pharmacology*, 61(3), 490P–491P.
- Cury, K., & Uchida, N. (2010). Robust Odor Coding via Inhalation-Coupled Transient Activity in the Mammalian Olfactory Bulb. *Neuron*, 68(3), 570–585.
- Dayan, P. and Abbott, L.F. (2001) Theoretical Neuroscience: Computational and Mathematical Modeling of Neural Systems. The MIT Press, Cambridge.
- Diodato, A., de Brimont, M., Yim, Y., Derian, N., Perrin, S., Pouch, J., ... Fleischmann, A. (2016). Molecular signatures of neural connectivity in the olfactory cortex. *Nature Communications*, 7, 12238.
- Millman, D., & Millman, D., & Murthy, V. (2020). Rapid Learning of Odor–Value Association in the Olfactory Striatum. *The Journal of Neuroscience*, 4335–4347.
- Draft, R., McGill, M., Kapoor, V., & Murthy, V. (2018). Carpenter ants use diverse antennae sampling strategies to track odor trails. *Journal of Experimental Biology*, jeb185124.
- Erskine, A., Bus, T., Herb, J., & Schaefer, A. (2019). AutonoMouse: High throughput operant conditioning reveals progressive impairment with graded olfactory bulb lesions. *PLOS ONE*, e0211571.
- Ferdenzi, C., Poncelet, J., Rouby, C., & Bensafi, M. (2014). Repeated exposure to odors induces affective habituation of perception and sniffing. *Frontiers in Behavioral Neuroscience*, 8, 119.

- Franks, K., Russo, M., Sosulski, D., Mulligan, A., Siegelbaum, S., & Axel, R. (2011). Recurrent Circuitry Dynamically Shapes the Activation of Piriform Cortex. *Neuron*, 49–56.
- Giessel, A., & Datta, S. (2014). Olfactory maps, circuits and computations. *Current Opinion in Neurobiology*, 24(1), 120–32.
- Gire, D. H., Kapoor, V., Arrighi-Allisan, A., Seminara, A., & Murthy, V. N. (2016). Mice Develop Efficient Strategies for Foraging and Navigation Using Complex Natural Stimuli. *Current Biology*, 26(10), 1261–1273.
- Godfrey, P., Malnic, B., & Buck, L. (2004). The mouse olfactory receptor gene family. *Proceedings of the National Academy of Sciences of the United States of America*, 2156–2161.
- Gold, J., & Shadlen, M. (2007). The Neural Basis of Decision Making. *Annual Review of Neuroscience*, 30(1), 535–574.
- Green, & Swets. (1966). Signal detection theory and psychophysics.
- Grimaud, J., & Murthy, V. (2018). How to monitor breathing in laboratory rodents: a review of the current methods. *Journal of neurophysiology*, 120(2), 624–632.
- Gupta, P., Albeanu, D., & Bhalla, U. (2015). Olfactory bulb coding of odors, mixtures and sniffs is a linear sum of odor time profiles. *Nature Neuroscience*, 18(2), 272–281.
- Hanks, T., Kopec, C., Brunton, B., Duan, C., Erlich, J., & Brody, C. (2015). Distinct relationships of parietal and prefrontal cortices to evidence accumulation. *Nature*, 520(7546), 220.

- Jun, J., Steinmetz, N., Siegle, J., et al. (2017). Fully integrated silicon probes for high-density recording of neural activity. *Nature*, 232–236.
- Kepecs, A., Uchida, N., & Mainen, Z. (2006). The Sniff as a Unit of Olfactory Processing. *Chemical Senses*, 31(2), 167–179.
- Khan, A., Sarangi, M., & Bhalla, U. (2012). Rats track odour trails accurately using a multi-layered strategy with near-optimal sampling. *Nature Communications*, 3, 703.
- Kleene, S. (2008). The Electrochemical Basis of Odor Transduction in Vertebrate Olfactory Cilia. *Chemical Senses*, 33(9), 839–859.
- Klowden, M. (2008). *Physiological Systems in Insects (Second Edition)*, 597–642.
- Lánský, P., & Rospars, J.-P. (1998). Odorant concentration and receptor potential in olfactory sensory neurons. *Biosystems*, 131–138.
- mai, T., Sakano, H., & Vosshall, L. (2010). Topographic Mapping—The Olfactory System. *Cold Spring Harbor Perspectives in Biology*, 2(8), a001776.
- Masset, P., Ott, T., Lak, A., Hirokawa, J., & Kepecs, A. (2020). Behavior- and Modality-General Representation of Confidence in Orbitofrontal Cortex. *Cell*, 182(1), 112–126.
- McDermott, J. (2009). The cocktail party problem. *Current Biology*, R1024–R1027.
- Mendonça, A., Drugowitsch, J., Vicente, I., DeWitt, E., Pouget, A., & Mainen, Z. (2020). The impact of learning on perceptual decisions and its implication for speed-accuracy tradeoffs. *Nature Communications*, 11(1), 2757.



- Minderer, M., Harvey, C., Donato, F., & Moser, E. (2016). Neuroscience: Virtual reality explored. *Nature*, 533(7603), 324–325.
- Miura, K., Mainen, Z., & Uchida, N. (2012). Odor Representations in Olfactory Cortex: Distributed Rate Coding and Decorrelated Population Activity. *Neuron*, 74(6), 1087–1098.
- Mombaerts, P., Wang, F., Dulac, C., Chao, S., Nemes, A., Mendelsohn, M., ... Axel, R. (1996). Visualizing an Olfactory Sensory Map. *Cell*, 87(4), 675–686.
- Morcos, A., & Harvey, C. (2016). History-dependent variability in population dynamics during evidence accumulation in cortex. *Nature Neuroscience*, 19(12), nn.4403.
- Murthy, V. (2011). Olfactory Maps in the Brain. *Neuroscience*, 34(1), 233–58.
- Nagayama, S., Homma, R., & Imamura, F. (2014). Neuronal organization of olfactory bulb circuits. *Frontiers in Neural Circuits*, 8, 98.
- O'Keefe, J., & Recce, M. (1993). Phase relationship between hippocampal place units and the EEG theta rhythm. *Hippocampus*, 317–330.
- Odoemene, O., Pisupati, S., Nguyen, H., & Churchland, A. (2018). Visual evidence accumulation guides decision-making in unrestrained mice. *Journal of Neuroscience*, 3478–17.
- Pachitariu, M., Steinmetz, N., Kadir, S., Carandini, M., & Harris, K. (2016). Kilosort: realtime spike-sorting for extracellular electrophysiology with hundreds of channels. *bioRxiv*, 061481.

- Pifferi, S., Menini, A., & Kurahashi, T. (2009). *The Neurobiology of Olfaction. Frontiers in Neuroscience* (Vol. 20092457, pp. 203–224).
- Pinto, L., Koay, S., Engelhard, B., Yoon, A., Deverett, B., Thiberge, S., Brody, C. (2018). An Accumulation-of-Evidence Task Using Visual Pulses for Mice Navigating in Virtual Reality. *Frontiers in Behavioral Neuroscience*, 12, 36.
- Radvansky, B., & Dombeck, D. (2018). An olfactory virtual reality system for mice. *Nature Communications*, 839.
- Ratcliff, R., & McKoon, G. (2008). The Diffusion Decision Model: Theory and Data for Two-Choice Decision Tasks. *Neural Computation*, 20(4), 873–922.
- Ressler, K., Sullivan, S., & Buck, L. (1994). Information coding in the olfactory system: Evidence for a stereotyped and highly organized epitope map in the olfactory bulb. *Cell*, 79(7), 1245–1255.
- Riffell, J., Shlizerman, E., Sanders, E., Abrell, L., Medina, B., Hinterwirth, A., & Kutz, N. (2014). Flower discrimination by pollinators in a dynamic chemical environment. *Science*, 344(6191), 1515–1518.
- Runyan, C., Piasini, E., Panzeri, S., & Harvey, C. (2017). Distinct timescales of population coding across cortex. *Nature*, 92–96.
- Saibene, F., Mognoni, P., Lafortuna, C., & Mostardi, R. (1978). Oronasal breathing during exercise. *Pflügers Archiv*, 378(1), 65–69.

- Scott, B., Constantinople, C., Akrami, A., Hanks, T., Brody, C., & Tank, D. (2017). Fronto-parietal Cortical Circuits Encode Accumulated Evidence with a Diversity of Timescales. *Neuron*, *95*(2), 385–398.
- Scott, B., Constantinople, C., Erlich, J., Tank, D., & Brody, C. (2015). Sources of noise during accumulation of evidence in unrestrained and voluntarily head-restrained rats. *eLife*, *4*, e11308.
- Serizawa, S., Miyamichi, K., & Sakano, H. (2004). One neuron–one receptor rule in the mouse olfactory system. *Trends in Genetics*, *20*(12), 648–653.
- Sherman, D., Worrell, J., Cui, Y., & Feldman, J. (2015). Optogenetic perturbation of preBötzing complex inhibitory neurons modulates respiratory pattern. *Nature Neuroscience*, *18*(3), 408–414.
- Shusterman, R., Smear, M., Koulakov, A., & Rinberg, D. (2011). Precise olfactory responses tile the sniff cycle. *Nature Neuroscience*, *14*(8), 1039.
- Slotnick, B. (2001). Animal cognition and the rat olfactory system. *Trends in Cognitive Sciences*, 216–222.
- Soucy, E., Albeanu, D., Fantana, A., Murthy, V., & Meister, M. (2009). Precision and diversity in an odor map on the olfactory bulb. *Nature Neuroscience*, 210–220.
- Stock, J. B., & Baker. (2009). *Encyclopedia of Microbiology (Third Edition)*, 71–78.
- Tolooshams, B., Song, A., Temereanca, S. & Ba, D.. (2020). Convolutional dictionary learning based auto-encoders for natural exponential-family distributions. *Proceedings of the 37th*

*International Conference on Machine Learning, in Proceedings of Machine Learning Research*, 119:9493-9503

Tsao, A., Sugar, J., Lu, L., Wang, C., Knierim, J., Moser, M.-B., & Moser, E. (2018). Integrating time from experience in the lateral entorhinal cortex. *Nature*, 57–62.

Urai, A., de Gee, J., Tsetsos, K., & Donner, T. (2019). Choice history biases subsequent evidence accumulation. *eLife*, e46331.

Vassar, R., Chao, S., Sitcheran, R., Nun˜ez, J., Vosshall, L., & Axel, R. (1994). Topographic organization of sensory projections to the olfactory bulb. *Cell*, 79(6), 981–991.

Vergassola, M., Villermaux, E., & Shraiman, B. (2007). “Infotaxis” as a strategy for searching without gradients. *Nature*, 445(7126), nature05464.

Verhagen, J., Wesson, D., Netoff, T., White, J., & Wachowiak, M. (2007). Sniffing controls an adaptive filter of sensory input to the olfactory bulb. *Nature Neuroscience*, 10(5), 631–639.

Wachowiak, M. (2011). All in a Sniff: Olfaction as a Model for Active Sensing. *Neuron*, 962–973.

Wachowiak, M. (2011). All in a Sniff: Olfaction as a Model for Active Sensing. *Neuron*, 962–973.

Walker, J., & O’Connell, R. (1986). Computerized odor psychophysical testing in mice. *Chemical Senses*, 439–453.

- Wallis, J. (2007). Orbitofrontal Cortex and Its Contribution to Decision-Making. *Annual Review of Neuroscience*, 31–56.
- Wang, C., Chen, X., Lee, H., Deshmukh, S., Yoganarasimha, Savelli, F., & Knierim, J. (2018). Egocentric coding of external items in the lateral entorhinal cortex. *Science*, 945–949.
- Waters, R. (1936). Carbon Dioxide Absorption from Anæsthetic Atmospheres. *Journal of the Royal Society of Medicine*, 30(1), 11–22.
- White, J. (2002). Encyclopedia of the Human Brain. 1–12.
- Willis, M., & Arbas, E. (1991). Odor-modulated upwind flight of the sphinx moth, *Manduca sexta* L. *Journal of Comparative Physiology A*, 427–440.
- Wilson, & McNaughton. (1993). Dynamics of the hippocampal ensemble code for space. *Science*, 1055–1058.
- Wilson, D., & Sullivan, R. (2011). Cortical Processing of Odor Objects. *Neuron*, 72(4), 506–19.
- Yartsev, M., Hanks, T., Yoon, A., & Brody, C. (2018). Causal contribution and dynamical encoding in the striatum during evidence accumulation. *eLife*, 7.
- Youngentob, S., Mozell, M., Sheeche, P., & Hornung, D. (1987). A quantitative analysis of sniffing strategies in rats performing odor detection tasks. *Physiology & Behavior*, 41(1), 59–69.

Zak, J., Reddy, G., Vergassola, M., & Murthy, V. (2020). Antagonistic odor interactions in olfactory sensory neurons are widespread in freely breathing mice. *Nature Communications*, 3350.